Studies on the Structural Mechanism of Iron Uptake and Release in Ovotransferrin N-Lobe

Kimihiko Mizutani

2001

Studies on the Structural Mechanism of Iron Uptake and Release in Ovotransferrin N-Lobe

Kimihiko Mizutani

2001

CONTENTS

ABBREVIATIONS

BisTris	2-[bis(2-hydroxyethyl)amino]-2-(hydroxymetyl)-propane-1,3 diol
CD	circular dichroism
MALDI-TOF-MS	matrix-assisted laser desorption/ionization time-of-flight mass spectrometry
NTA	nitrilotriacetate
PAGE	polyacrylamide gel electrophoresis
SDS	sodium dodecyl sulfate
Trf	transferrin

INTRODUCTION

Transferrins are a homologous group of iron (Fe^{3+})-binding proteins that include serum transferrin, ovotransferrin and lactoferrin (Aisen et al., 1980). They are ~80 kDa single-chain bilobe proteins possessing one Fe^{3+} binding site in each lobe. X-ray crystallographic data for the diferric forms of lactoferrin (Sharma et al., 1999a; Anderson et al., 1989), serum transferrin (Bailey et al., 1988), and ovotransferrin (Kurokawa et al., 1995; Rawas et al., 1996) have demonstrated that the N- and C- lobes have similar tertiary structures. Each lobe is made up of a pair of domains (domain 1 and domain 2); domain 1 is comprised of two non-contiguous regions (domain 1N and domain 1C), though domain 2 is a contiguous portion of the chain. The two Fe^{3+} binding sites are located within the interdomain cleft of each lobe. Four of the six Fe^{3+}-coordination sites are occupied by the side chains of amino acid residues and the remaining two by a synergistic anion, physiologically bicarbonate. The crystallographic data also demonstrate that four Fe^{3+}-coordinating amino acid residues (Asp60, Tyr92, Tyr191 and His250 in the N-lobe of ovotransferrin) are all conserved in both the lobes of serum transferrin, ovotransferrin and lactoferrin.

These proteins serve to control the levels of iron in the body fluids of vertebrates via their ability to bind two Fe^{3+} ions together very tightly with two CO_3^{2-} anions (Aisen & Listowsky, 1980). Serum transferrin and ovotransferrin can act as an iron transporter to target cells. The transferrin-dependent Fe^{3+} delivery to the target cells occurs in such a way that the diferric transferrin first binds with the specific receptor that resides on the plasma membrane (Klausner et al., 1983). The transferrin- receptor complex is then internalized into the cell, and the complex releases Fe^{3+} at acidic pH in the endosome

(Klausner et al., 1983).

The N lobe of ovotransferrin can be isolated after mild proteolysis (Oe et al., 1988). It consists of a single polypeptide chain of 332 amino acid residues and has a molecular mass of approximately 36 kDa. In Chpater 1, the author prepared the N-terminal subdomain fragment of ovotransferrin N-lobe and anlyzed its structural characteristeics. In Chapter 2-4, the author determined crystal structures of iron-loaded open form, apo-form, and holo-form of ovotransferrin N-lobe. In Chapter 4 the detailed structural mechanism of iron uptake and release in transferrins was discussed using the crystal structures.

CHAPTER 1

Preparation of the N-terminal Subdomain Fragment of Ovotransferrin and Its Structural Characteristics

Structure and function of transferrins are maintained by many intrachain disulfide bonds. Among the six lobes of the transferrin group, ovotransferrin N lobe contains the least number of intrachain disulfides of six. Two disulfide bonds (SS-I/Cys10-Cys45 and SS-II/Cys20-Cys36) are included in Domain 1 and the other four disulfide bonds (SS-III/Cys115-Cys197, SS-IV/Cys160-Cys174, SS-V/Cys171-182, SS-VI/Cys228-Cys242) are contained in Domain 2 (Fig. 1) (Dewan et al., 1993).

Partially disulfide reduced ovotransferrin N lobe with 4, 3 or 2 disulfide bonds was isolated after reduction with dithiothreitol under nondenaturing condition (Yamashita et

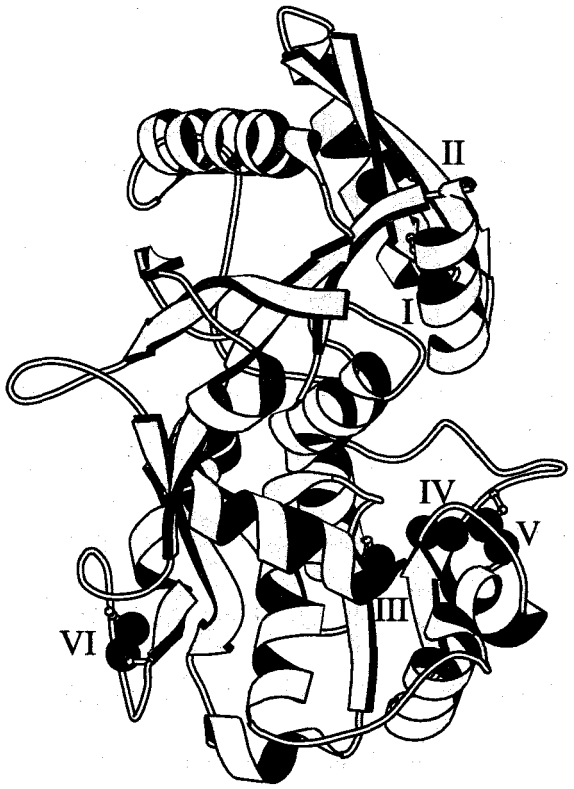

Fig. 1. Schematic view of ovotransferrin N lobe.
The figure was drawn based on the X-ray crystallographic data of iron-loaded ovotransferrin N lobe (Dewan et al., 1993) using the program MolScript (Kraulis, 1991). The small filled circles represent the sulfur atoms that are involved in disulfide bonds (I-VI).

al., 1995). Two disulfide bonds were not reduced under this condition. Partially disulfide reduced ovotransferrin N lobe with 4 disulfide bonds retains the iron-binding capacity though partially disulfide reduced ovotransferrin N lobe with 3 or 2 disulfide bonds has no iron-binding capacity. Both of two disulfide bonds that were not reduced are included in N terminal part of domain 1. Thus the author speculated the fragments corresponding to N terminal part of domain 1 were able to prepared from disulfide reduced ovotransferrin N lobe with 2 disulfide bonds by proteolysis.

In this chapter, a fragment was isolated after proteolysis of partially disulfide reduced ovotransferrin N lobe with 2 disulfide bonds, indicating that N terminal part of the partially disulfide reduced ovotransferrin has resistance to the proteolysis. The author investigated the molecular property of the fragment and proved that the fragment corresponds to N terminal subdomain (N terminal part of domain 1) of ovotransferrin. Far UV CD spectrum of the fragment indicated that it had secondary structure.

EXPRERIMENTAL PROCEDURE

Materials. Ovotransferrin N lobe (the N-terminal half-molecule, Ala1-Arg332) was prepared as described by Oe et al. (1988). The two-disulfide form of ovotransferrin N lobe was prepared according to the protocol described by Yamashita et al. (1995). Shortly, protein disulfides were reduced under non-denatureing conditions by incubating the isolated ovotrasnferrin N lobe at 1.0 mg/ml and 6 °C with 10 mM dithiothreitol for 19 hours in 0.1 M Tris-HCl buffer, pH 8.0 containing 0.1 mM Na-EDTA. The protein was alkylated with 0.1 M iodoacetic acid at 37 °C for 15 minutes. The sample was dialyzed against 50 mM Tris-HCl buffer, pH 8.0. Chymotrypsin and soybean trypsin inhibitor were purchased from Sigma. Carboxypeptidase Y was purchased from

Oriental Yeast. Soybean trypsin inhibitor was immobilized onto Affi-Gel 10 (Bio-RAD) as directed by the manufacturer. Other Chemicals were guaranteed grade from Nacalai Tesque.

Limited proteolysis and fragment purification. Intact ovotransferrin N lobe or the two difulfide form of ovotransferrin N lobe was digested at 0.429 μg/μl in 50 mM Tris-HCl buffer, pH 8.0, at 4 °C for various times with chymotrypsin at a protein to enzyme ratio of 50:1 (w/w). Proteolysis was terminated by the addition of 1/14 volume of 1N HCl and samples corresponding to 3 μg of the original protein were analyzed by SDS-PAGE according to the method described by Schagger and Jagow (1987) using 16.5 % polyacrylamide gel. The gel was electroblotted on to polyvinylidene difluoride membranes as described (Hirano, 1989). The bands corresponding to 8 kDa fragment and 11 kDa fragment were excised and their N terminal sequences were analyzed with a protein sequenator (Applied Biosystems model 477A/120A). For purification of 8 kDa fragment, the two disulfide protein was digested for 60 minutes in the same way and then the proteolytic reaction was terminated by passing the sample through a immobilized trypsin-inhibitor column (1.5 x 1.5 cm) equibrated with distilled water. The sample was diluted 5-fold with distilled water, and applied to an ion-exchange column (Mono Q HR 5/5, Pharmacia LKB Biotechnology Inc.) equibrated with 10 mM Tris-HCl buffer, pH 8.0, and connected to a HPLC apparatus (Shimadzu, LC-10A). Fragments were eluted with a linear gradient (10-250 mM Tris-HCl buffer, pH 8.0) and peak fractions were analyzed by SDS-PAGE in the same way. A peak fraction containing 8 kDa fragment was collected and the fragment was further purified by rechromatography under the same HPLC conditions.

Chemical Analyses. The N terminal amino acid sequence of the purified 8 kDa

fragment was determined with the protein sequenator. The C terminal amino acid sequence of the fragment was analyzed by sequential digestion with carboxypeptidase Y. The fragment was denatured by incubation in 25 mM Tris-HCl buffer, pH 7 containing 8 M urea at room temperature for 15 minutes and the sample was diluted with 5 volume of 25 mM Tris-HCl, pH 7. The fragment was digested with carboxypeptidase Y at 30 °C for various times at protein to enzyme molar ratio of 30:1. Aliquots of the digestion mixture were diluted with 43 volume of 0.2 M sodium citrate buffer, pH 2.2. Released amino acids were quantified with an amino acid analyzer (Hitachi amino acid analyzer, Type-835).

Amino acid composition was analyzed with the amino acid analyzer after hydrolysis of the fragment with 3 N mercaptoethanesulfonic acid for 22 hours at 110 °C. For the determination of cystein residues the fragment was reduced with 30 mM dithiothreitol in 100 mM Tris-HCl, pH 8.0, containing 9 M urea at 37 °C for one hour or with 30 mM dithiothreitol in 100 mM Tris-HCl, pH 8.0, at 6 °C for 5 hours. Reduced samples were alkylated with 100 mM monoiodoacetic acid, and hydrolyzed in the same way. The carboxtmethyl cysteine was determined with the amino acid analyzer in the same way.

Molecular mass determination. The molecular mass of the fragment was determined using MALDI-TOF-MS (PerSeptive Biosystems, Voyager RP).

Measurement of CD Spectra. The purified 8 kDa fragment dissolved at 0.06 mg/ml in 80 mM Tris-HCl, pH 8.0, was analyzed for the far UV CD spectrum at 6 °C with a spectropolarimeter (Jasco, J-720) using a cuvette of 0.1 cm light path. The far UV CD spectrum of disulfide reduced and denatured form, incubated in Tris-HCl buffer, pH 8.0, containing 7 M urea and 30 mM dithiothreitol. The duplicate data were averaged and expressed as mean residue ellipticity.

Computation of Accessibility of Sulfur Atoms. Accessibility of sulfur atoms was calculated using program Naccess (Hubbard & Thornton, 1987) with X-ray crystallographic data. Naccess is an implementation of the method of Lee and Richards (1971).

RESULTS

Time course of proteolytic digestion. To obtain structural information about ovotransferrin N lobe, disulfide-intact and two disulfide proteins were digested with chymotrypsin, and the time course of digestion was monitored by SDS-PAGE. As shown in Fig. 2., the two disulfide form was more extensively digested than the disulfide-intact form: at a prolonged incubation time of 64 minutes, two fragments with molecular masses of 19 kDa and 12 kDa were accumulated upon the digestion of the disulfide-intact form, while two fragments with molecular masses of about 8 kDa and 11 kDa were produced from the two-disulfide form of ovotransferrin N lobe (Fig. 2).

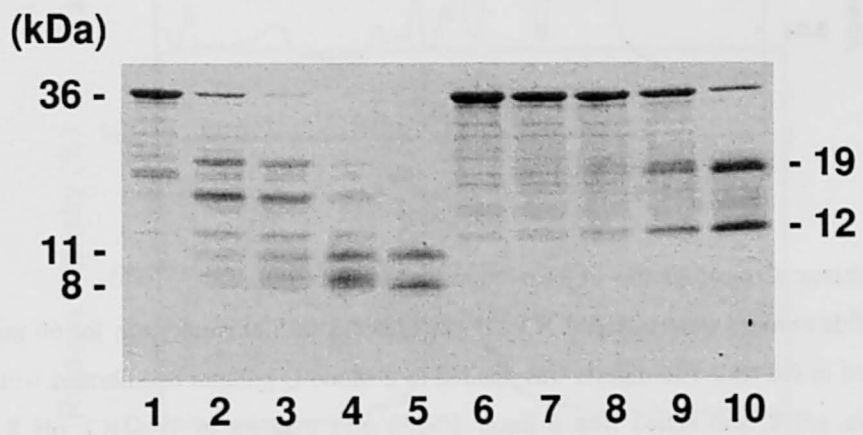

Fig. 2. Chymotrypsin digestion of partially disulfide reduced ovotransferrin N lobe.

Partially disulfide reduced ovotransferrin N lobe with two disulfide bonds (lanes 1-5) and non-reduced ovotransferrin N lobe (lanes 6-10) were digested with chymotrypsin for 0 min (lane 1 and 6), 1 min (lane 2 and 7), 4 min (lane 3 and 8), 16 min (lane 4 and 9) and 64 min (lane 5 and 10) and

Data showed that both of the fragments were consisted of N terminal acid sequence of Ala-Pro-Pro-. According to the established primary structure of ovotransferrin (Williams et al., 1982), this sequence was consistent with the N terminal sequence of intact ovotransferrin. The author also observed that in the trypsin digestion of the two-disulfide form of ovotransferrin N lobe, two fragments with similar molecular masses of 11 and 9 kDa are produced. It is therefore very likely that the native conformation is retained in a N-terminal region of the two-disulfide form of the N lobe.

Purification of 8 kDa fragment. To investigate more exactly the structural characteristics of the 8 kDa fragment, the author purified the fragment. The two-disulfide form of ovotransferrin N lobe was digested with chymotrypsin. The digests

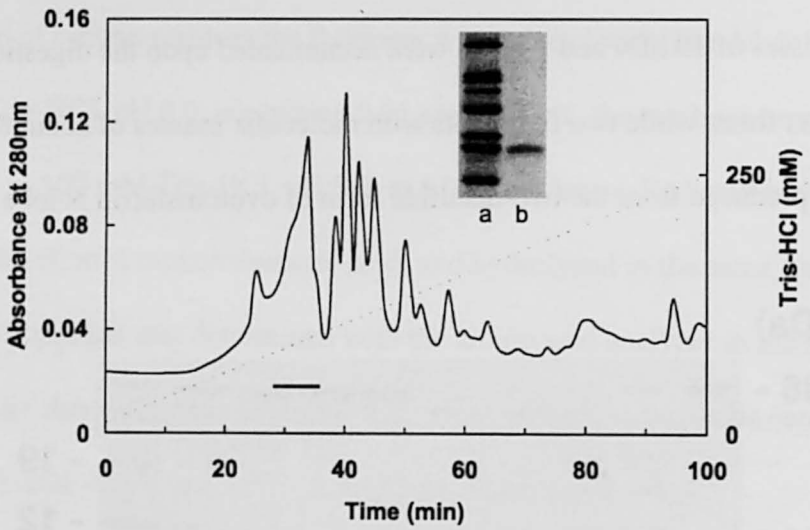

Fig. 3. Ion-exchange chromatography of the ovotransferrin N lobe digest.

Partially disulfide reduced ovotransferrin N lobe was digested with chymotrypsin for 60 minutes on ice as described in the text. The digests was applied to a Mono-Q column equilibrated with 10 mM Tris-HCl buffer, pH 8, and eluted with a linear 10-250 mM gradient of Tris-HCl, pH 8, for 100 minutes and detected by measuring the absorption at 280 nm. The peak indicated by the bar was collected. In the inset, the purified fragment and standard proteins (carbonic anhydrase, 31.0 kDa; soybean trypsin inhibitor, 20.5/19.8 kDa; horse heart myoglobin, 16.7 kDa; lysozyme, 14.4 kDa; myoglobin fragment F1, 8.1 kDa; myoglobin fragment F2, 6.2 kDa; myoglobin fragment F3, 2.5 kDa) were analyzed by SDS-PAGE.

were applied to an ion-exchange column and eluted as shown in Fig. 3. SDS-PAGE analysis for the peak fractions revealed that a peak with a retention time of 34 minutes contained 8 kDa fragment (data not shown). The fragment was further purified by rechromatography in the same way and a peak fraction was collected. The sample showed a single band on SDS-PAGE (Fig.3, inset). The recovery of the purified 8 kDa fragment as determined by amino acid analyses was about 7 %.

Assignment for the primary structure. To assign the primary structure, the author determined the N- and C-terminal sequences of the 8 kDa fragment. The N terminal amino acid sequence, determined with protein sequenator, was again Ala-Pro-Pro-, indicating that the fragment is the one containing the sequence of intact ovotransferrin.

The C terminal amino acid sequence of the fragment was determined by digestion with carboxypeptidase Y. Tyr and Pro were released first and then Ala and Leu were released. The release of Gly and Glu was followed. In the light of the known primary structure, this profile was consistent with the view that the C terminus of the fragment is

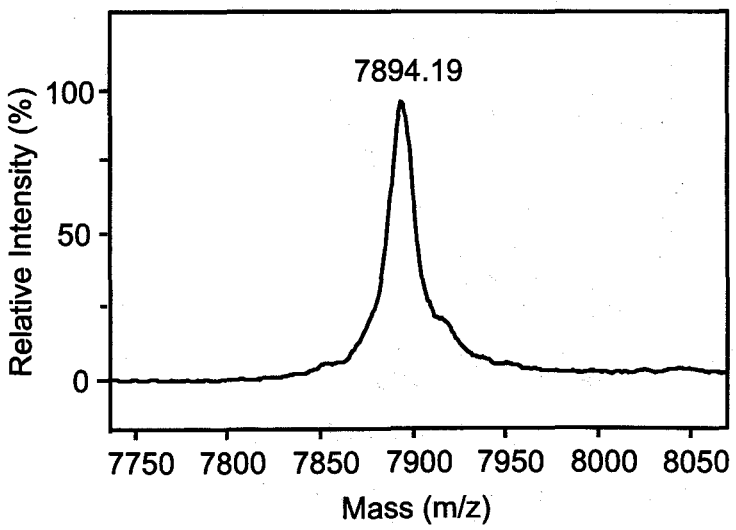

Fig. 4. Molecular Mass Determination of the 8-kDa Fragment. The molecular mass of the purified 8-kDa fragment was determined by MALDI-TOF-MS

Tyr72. To determine more exactly the C-terminus, the molecular mass of the fragment was determined with MALDI-TOF-MS. As shown in Fig. 4., the molecular mass of the fragment was 7893.19. This value was almost exactly the same as the theoretical molecular mass of 7895.00 for the fragment, Ala1 to Tyr72.

From the N and C terminal sequence and molecular mass, the fragment was assigned exactly to the sequence of Ala1-Tyr72, which corresponds to N terminal subdomain of ovotransferrin. This conclusion was further confirmed by the amino acid analysis.

CD spectra. To obtain conformational information about the purified 8 kDa fragment, the author compared far UV CD spectra of the fragment in the presence and absence of high concentration of urea. As shown in Fig. 5., the spectrum of the fragment was very similar to that of intact ovotransferrin N lobe, while the far UV CD spectrum of the fragment showed a typical profile for a denatured protein. These data indicate that the fragment retain some folded conformation. As shown in Table 1, the amino acid

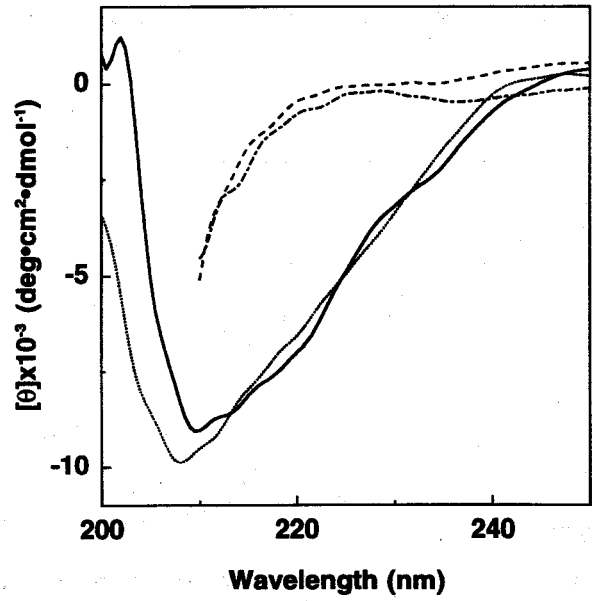

Fig. 5. Far-UV CD Spectrum of the N terminal 8 kDa fragment.

The far-UV CD spectra of ovotransferrin N lobe (dotted line), N terminal 8 kDa fragment (solid line) and reduced and denatured fragment (broken line) were measured as described in the text.

composition of the fragment was consistent with in an experimental error with theoretical amino acid composition for the 8 kDa fragment of Ala1-Tyr72 in ovotransferrin.

Disulfide bonds in the fragment. The 8 kDa fragment should contain two intrachain disulfide bonds of SS-I (Cys-10-Cys45) and SS-II (Cys20-Cys36); both of them have been shown to be in accessible for dithiothreitol in the intact form of ovotransferrin N lobe. To investigate the disulfide state, the fragment was reduced and alkylated in the presence and absence of urea, and then cystein residues were determined as carboxymethyl cysteine. As summarized in Table 2, the number of carboxymethyl cysteine was 3.4 for the fragment reduced under denaturing conditions. In contrast, no carboxymethyl cysteine was detected, when the fragment was alkylated without reduction in the absence of urea. This indicates that the two disulfide bonds are intact in the fragment. The number of carboxymethyl cysteine observed in the sample reduced

Table 1
Amino acid compositions of N terminal 8 kDa fragment and N2 fragment

	N terminal 8 kDa fragment	
amino acid	experimental[a]	theoretical
Ala	7.9	8
Arg	3.0	3
Asx	7.9	8
Cys[b]	3.4	4
Glx	8.2	9
Gly	3.5	3
His	0.0	0
Ile	4.9	6
Leu	6.4	6
Lys	5.5	5
Met	0.0	0
Phe	2.1	1
Pro	4.0	4
Ser	5.5	5
Thr	3.9	4
Trp	0.9	1
Tyr	1.9	2
Val	2.9	3
total	71.6	72.0

[a] Normalized with molecular weight

[b] Determined as carboxymethyl cystein

Table 2
Measurement of Carboxymethyl Cysteine

Conditions*	Dithiothreitol (mM)	Carboxymethyl Cysteine
D	30	3.4
N	—	0
N	30	3.5

*Conditions for disulfide reduction and alkylation with iodoacetic acid. D and N represent in the presence and absence of 9 M urea.

and alkylated under nondenaturing conditions. This indicate that disulfide bonds in the fragment are easy to be reduced in an exposed state.

DISCUSSION

In this chapter, partially disulfide reduced ovotransferrin N lobe with two disulfide bonds was digested with chymotrypsin and two N terminal fragments were observed on SDS-PAGE. The author purified a fragment with ion-exchange chromatography and on SDS-PAGE, no contaminant peptide fragment was detected. To assign primary structure, N- and C- terminal sequence and molecular mass of the purified fragment was determined. N terminal sequence of the fragment was same as that of ovotransferrin N lobe and data from C terminal analysis of the fragment strongly suggest that the fragment is corresponding to Ala1-Tyr72 in ovotransferrin. Measured molecular mass of the fragment was nearly equal to that of Ala1-Tyr72 fragment. Thus it was exactly decided that the fragment is Ala1-Tyr72; N terminal subdomain (N terminal part of domain 1) of ovotransferrin. This fragment contains all of the disulfide bonds in the original partially disulfide reduced ovotransferrin N lobe with 2 disulfide bonds and has an iron-coordinating residue Asp60. Far UV CD spectrum of the N terminal 8 kDa fragment indicated that the fragment has secondary structure. It also suggests that fragmentation by chymotrypsin induced no drastic alteration in the conformation and N

terminal subdomain is folded in original partially disulfide reduced ovotransferrin N lobe.

Amino acid composition of the fragment was determined using amino acid analyzer. The data nearly agreed with assigned primary structure. In this analysis, it was also indicated that both of two disulfide bonds in the fragment is easy to be reduced under nondenaturing condition, though two disulfide bonds (SS-I and SS-II) in original ovotransferrin N lobe were not reduced under same condition. To know mechanism for this fact, accessibility of sulfur atoms was computed (Table 3). In ovotransferrin N lobe, accessibility of sulfur atoms in Cys171 participating in SS-V is high, supporting the fact, described by Yamashita et al. (1995), that SS-IV and SS-V were reduced first with dithiothreitol under nondenaturing condition. In N terminal 8 kDa fragment, accessibility of a sulfur atom in Cys20 participating in SS-II is high, indicating that the fragment became easy to be reduced since peptide chain in ovotransferrin covering Cys20 was removed by fragmentation (Fig. 6).

Table 3
Accessibility of sulphur atoms

This data were calculated with the program Naccess.

S-S	Cysteines	Accessible surface area (Å^2)	
		N-OVT	8kDa fragment
I	Cys10	0.0	0.0
	Cys56	0.0	0.0
II	Cys20	0.4	3.0
	Cys36	0.0	0.0
III	Cys115	0.0	—
	Cys197	0.0	—
IV	Cys160	0.1	—
	Cys174	0.0	—
V	Cys171	9.7	—
	Cys182	0.0	—
VI	Cys228	0.0	—
	Cys242	0.1	—

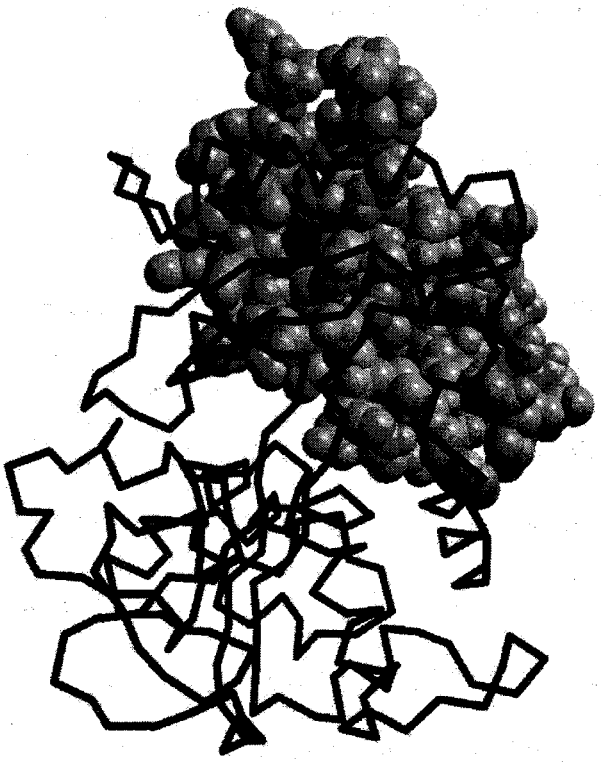

Fig. 6. View of the N terminal 8 kDa fragment with rest of ovotransferrin N lobe.
Atoms in N terminal 8 kDa fragment are shown in space-filling representation. A black tube represents the polypeptide backbone as a series of bonds connecting the adjacent alpha carbons in rest of ovotransferrin N lobe (residues 73-341). Black spheres represents sulfurs in cystine. This figure was generated with the program MolScript and Raster3D (Merritt & Murphy, 1994).

To study protein function, protein fragmentation approaches have been used for many proteins. This approach was used for ovotransferrin in previous studies. C terminal peptide fragment (OTFN6) corresponding to C terminal part of domain 1 was prepared and used to indicate it is important to stabilize iron-bound form (Kurokawa et al., 1994). The fragment corresponding to domain 2 was also prepared and used to study iron-binding mechanism. In this study, it was suggested that N terminal subdomain (N terminal part of domain 1) and iron-coordinating ligand in the subdomain plays significant key role for domain closure in iron uptake. This mechanism must be certified by using of the fragment corresponding to N terminal part of domain 1. Up to now the fragment had not been prepared, but the author prepared the fragment containing a iron-coordinating residue Asp 60. This fragment will be greatly useful to study iron-binding mechanism.

CHAPTER 2

Crystal Structure of Iron-loaded but Domain-opened Ovotransferrin N-Lobe

Crystal structures of the diferric forms (Bailey et al., 1988; Anderson et al., 1989; Kurokawa et al., 1995; Rawas et al., 1996; Moore et al., 1997) and the monoferric N-lobes (Sarra et al., 1990; Dewan et al., 1993; Day et al., 1993; MacGillivray et al., 1998) of several transferrins reveal that the two domains are closed over an Fe^{3+} ion. For the iron-free apo form, however, x-ray crystallographic (Anderson et al., 1990; Rawas et al., 1997; Jeffrey et al., 1998) and solution scattering (Grossmann et al., 1992, 1993a, 1998; Mecklenburg et al., 1997) analyses have revealed that all of the transferrin lobes, except for the lactoferrin C-lobe in crystal, assume a conformation with an opening of the interdomain cleft. This implies that transferrin initially binds the Fe^{3+} ion in the open form before being transformed into the closed holo form (Baker et al., 1987; Baker & Lindley, 1992). Differential domain and hinge locations of the four protein ligands (Asp 60 in the domain 1, Tyr 191 in the domain 2, and Tyr 92 and His 250 in different hinges) (Bailey et al., 1988; Anderson et al., 1989; Kurokawa et al., 1995; Rawas et al., 1996; Moore et al., 1997; Sarra et al., 1990; Dewan et al., 1993; Day et al., 1993; MacGillivray et al., 1998) inevitably require an alternative Fe^{3+} coordination structure for the Fe^{3+} -loaded, domain-opened intermediate. Such an alternative structural state has been a central question to be solved for the understanding of the Fe^{3+} binding pathway in transferrin.

A major difficulty encountered in the structural analysis for the intermediate is to prepare a stable protein form that reasonably mimics it. One of the most promising ways

may be the site-directed mutagenesis approach for the amino acid residues that are implicated in the Fe^{3+} coordination. An Fe^{3+} -loaded, domain-opened transferrin form, however, has not been obtained so far by site-directed mutagenesis; either the Asp- or His-ligand mutant of the lactoferrin N-lobe assumes the holo-like closed conformation (Faber et al., 1996a; Nicholson et al., 1997). The mutant lactoferrin N-lobe in which the synergistic anion-binding residue, Arg 121, is replaced by the serine or glutamic acid residue also assumes the closed conformation (Faber et al., 1996b).

In this chapter, the author employed an alternative strategy using an apo crystal: the Fe^{3+} soaking conditions in which the colorless crystal turns red without any collapse were searched. As a successful condition, an apo crystal of ovotransferrin N-lobe was soaked with the Fe^{3+}·NTA complex in the absence of CO_3^{2-} , and then its structure was solved at a 2.1 Å resolution. The author reports a novel structural state of transferrin in this chapter: the Fe^{3+} -loaded structure of ovotransferrin N-lobe with essentially the same open conformation as the apo form. In this structure, the bound iron atom is coordinated by the two protein ligands of Tyr 92 -OH and Tyr 191 -OH. Other Fe^{3+} coordination sites are occupied by a NTA anion, which is stabilized through the hydrogen bonds with protein groups. The observation strongly suggests that the two tyrosine residues are the initial Fe^{3+} -binding ligands in the open transferrin.

EXPERIMENTAL PROCEDURES

Crystallization. The isolated N-lobe (N-terminal half-molecule) of hen ovotransferrin was purified as described (Oe et al., 1988). The apo form of the protein was crystallized using the hanging drop vapor diffusion method. A solution of a crystallization droplet was prepared on a siliconized coverslip by mixing 5 ml of protein

solution (44.4 mg/ml in 0.05 M BisTris-HCl buffer, pH 6.0) with 5 ml of precipitant solution (0.05 M BisTris buffer, pH 6.0, 52% ammonium sulfate). The droplets were equilibrated against 1 ml of the precipitant solution at 20 °C. Hexagonal apo crystals were obtained within 1 month. For Fe^{3+} soaking, the apo crystals were first transferred to a precipitant solution at higher pH (0.05 M BisTris-HCl buffer, pH 7.5, 52% ammonium sulfate) and then stepwise to raised precipitant concentrations (56, 62, 68, 74, and then 80% ammonium sulfate). The colorless crystals were incubated at 20 °C with 3.0 mM Fe^{3+} ·NTA for 4 h, thereby being transformed into red ones.

Data Collection and Processing. Diffraction data were collected using CuKα radiation (= 1.5418 Å) with a Siemens Hi-Star area detector coupled to a rotating anode generator (Mac Science M18XHF). The crystal of the Fe^{3+} -soaked form was found to belong to the same space group of $P6_322$ (Table 1) as that of the apo form. 188,024 reflections were collected to 2.09 Å. The data were processed, merged, and scaled with

Table 1
Summary of data collection and refinement

Crystal data	
Space group	$P6_322$
Cell dimensions	
a (Å)	125.29
b (Å)	125.29
c (Å)	87.53
V_m (Å^3/Da)	2.7
Molecules/asymmetric unit	1
Observed reflections	188,024
Resolution (Å)	2.09
Independent reflections	24,284
completeness (%)	100
R_{sym} (%)	7.9
Refinement statistics	
Resolution limits (Å)	7.0–2.10
No. of reflections used ($F > 2\sigma(F)$)	20,679
completeness (%)	88.3
No. of protein atoms	2,543
No. of solvent molecules	153
Ions	$3SO_4$/1Fe/1NTA
Final *R* factor	0.189
Free *R* value	0.256
Average *B* factor (Å^2)	22.2
Root mean square deviation from standard geometry	
Bond distances (Å)	0.014
Bond angles (degrees)	3.03
Dihedrals (degrees)	25.0
Improper dihedrals (degrees)	1.37

the SAINT program (Siemens Analytical x-ray Instruments, Inc., Madison, WI).

Model Building and Refinement. As the model structure, the author employed the apo structure of ovotransferrin N-lobe [chapter 3] that had been solved at 1.9 Å resolution by the isomorphous replacement method using the hexagonal apo crystals. Using the apo structure model and the diffraction data of the Fe^{3+} -soaked form, refinement calculations were carried out by X-PLOR (Brünger, 1993). One NTA molecule and one iron atom, which were identified from a clear difference density *(Fo - Fc)* map of the first refinement round, were included in the model, followed by more than 10 rounds of refinements and manual model buildings. The parameter and topology files of NTA for X-PLOR (24) were prepared after building and energy minimization of NTA by QUANTA and CHARM (Molecular Simulations Inc., San Diego, CA).

The omit maps (*2Fo - Fc*, contoured at 1 σ and *Fo - Fc*, contoured at 3 σ) were obtained using the reflection data of the Fe^{3+} -soaked form at 7.0-2.1 Å resolution after refinement of the model in which the NTA molecule was excluded. An anomalous difference Fourier density map contoured at 3 σ was calculated with a separate data set of the Fe^{3+} -soaked form at 7.0-2.1 Å resolution with pair completeness of 95.8% by the program PHASES. The phases were calculated from the final model without an iron atom by X-PLOR and merged with the data by PHASES.

RESULTS

Quality of the Final Model. The N-lobe of ovotransferrin comprises 332 amino acid residues (Oe et al., 1988). Residues 1-3, however, are not included in the final model because no clearly interpretable electron density could be seen for these residues. In the final *2Fo - Fc* electron density map, there is no break in the main chain density when

contoured at the 1 σ level. Relevant refinement statistics are given in Table 1. The overall completeness, *R* factor, and free-*R* value were 88.3%, 0.189, and 0.256, respectively, for the data more than 2 σ (*F*). For the highest resolution bin (2.10-2.19 Å), the completeness was 75.5%, and the *R* factor and free-*R* value were, respectively, 0.262 and 0.274. From a Luzzati plot, the mean absolute error in atomic position is estimated to be 0.24 Å.

A Ramachandran plot (Ramakrishnan & Ramachandran, 1965) of the main chain torsion angles is shown in Fig. 1; 88.3% of the residues are in the core regions, with 99.3% of the residues lying within the allowed regions as defined in the program PROCHECK (Laskowsky et al., 1993). As a non-glycine residue, Leu 299 lies outside the allowed regions ($\phi = 75.0°$, $\psi = 252.2°$). This leucine residue is the central residue in a γ-turn. The γ-turn of the equivalent leucine residue is the one con-served in all of the N- and C-lobes of serum transferrin (Bailey et al., 1988), ovotransferrin (Kurokawa

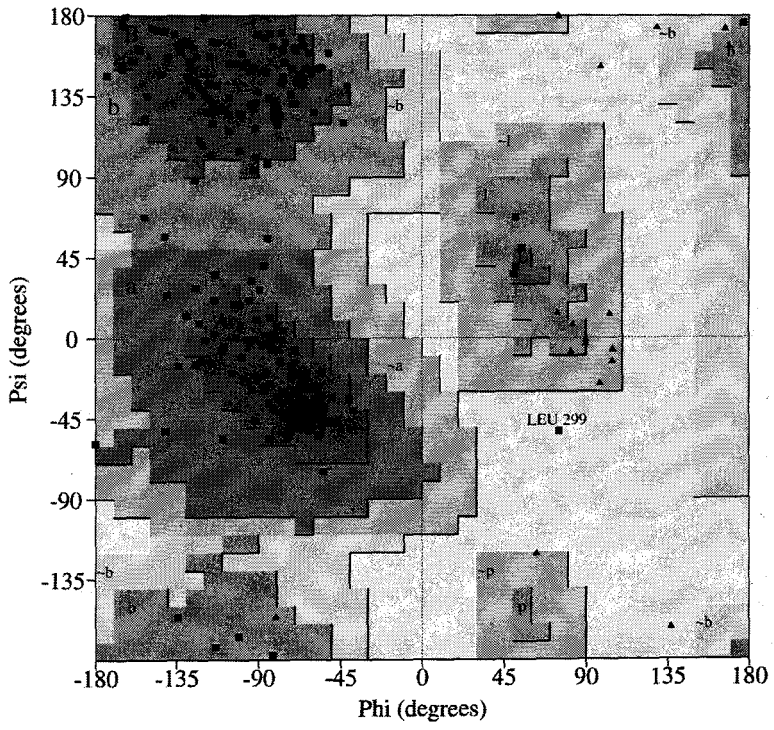

Fig.1. Ramachandran plot of the backbone torsion angles. Glycine residues are represented by triangles and non-glycine residues as squares. The γ-turn residue, Leu 299 , is labeled.

al., 1995), and lactoferrin (Moore et al., 1997).

Overall Organization of the Structure. Fig. 2 displays the overall structure of ovotransferrin N-lobe as a Cα trace. The overall structure of the Fe^{3+} -soaked form was almost exactly the same as that of the apo form. The root mean square deviation for 329 Cα atoms was only 0.19 Å. These structures, when compared with the holo (the Fe^{3+} - and CO_3^{2-} -loaded form) structure of ovotransferrin N-lobe (Dewan et al., 1993), comprise a domain-opened conformation (Fig. 2). The extent and mode of the opening were almost the same as in the N-lobes of the whole molecules of lactoferrin (Anderson et al., 1990) and duck (Rawas et al., 1997) and hen ovotransferrin (Kurokawa et al., 1999): as calculated by the rigid body motion method (Gerstein et al., 1993), the domains move 49.7° around a rotation axis passing through the .two β-strands linking the domains.

Another important observation in Fig. 2 is that an iron atom exists in the opened

Color figure shown in page 20-a

Fig.2.Stereo Cα plots of apo (black) and Fe^{3+} -soaked (cyan) and holo forms (red) of ovotransferrin N-lobe.

The figures are produced with MOLSCRIPT (Kraulis, 1993) and Raster3D (Merritt & Bacon, 1997) as the superimposed ones on domain 2. The holo (Fe^{3+} - and CO_3^{2-} -loaded ovotransferrin N-lobe) structure is drawn using the previous data (Dewan et al., 1993). The apo structure of ovotransferrin N-lobe is the one employed as the model for the current structural determination of the Fe^{3+} -soaked form (see "Experimental Procedures"). The residue numbers are labeled for the Fe^{3+} -soaked form. The iron atom (green sphere) and the side chains (blue)of His 250 , Asp 60 , Tyr 92 , and Tyr 191 (from top to bottom in this order) for the Fe^{3+} -soaked form are also displayed.

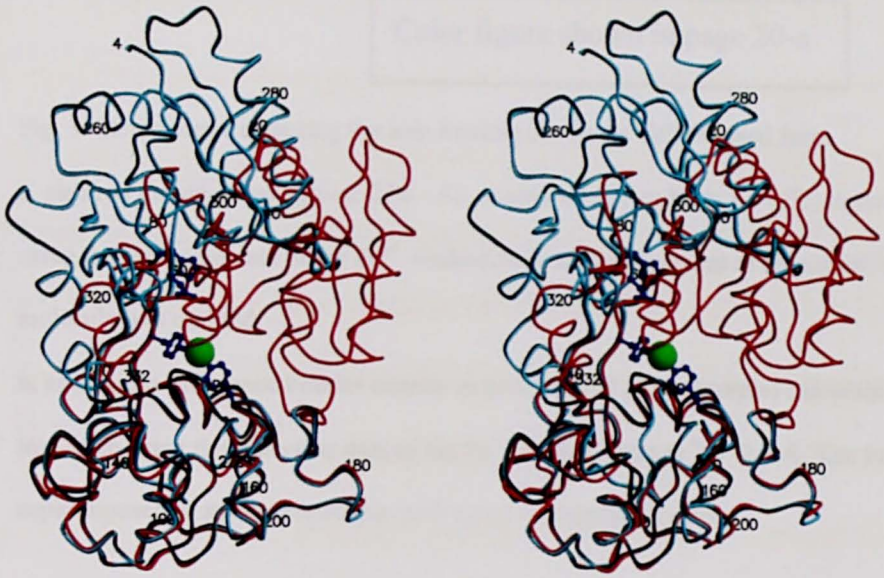

Fig. 2.

a

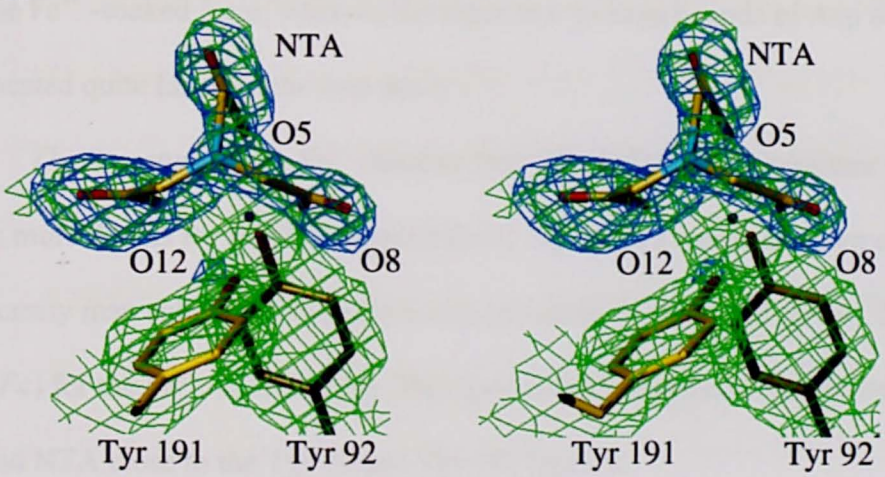

Fig. 3.

b

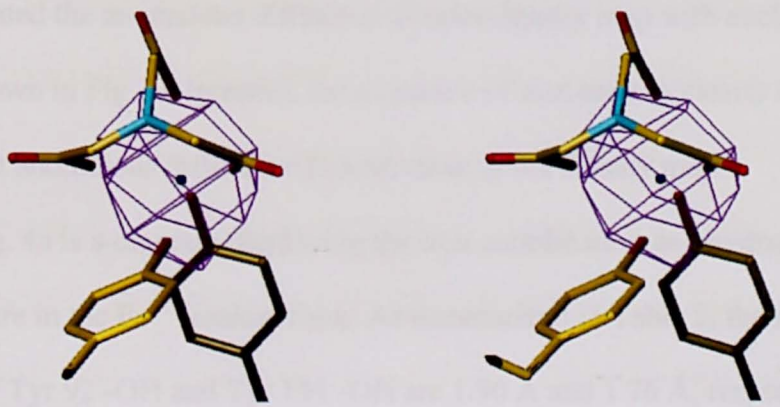

Color figure shown in page 20-a

Fig. 3. Stereo views depicting the iron binding site in the Fe^{3+} -soaked form.

a, electron density maps (green: *2Fo - Fc*, contoured at 1 σ; blue: *Fo - Fc*, contoured at 3 σ) obtained using the reflection data of the Fe^{3+} -soaked form after refinement of the model in which the NTA molecule was omitted.

b, anomalous difference Fourier density map contoured at 3 σ (purple) calculated with exclusion of an iron atom using the reflection data of the Fe^{3+} -soaked form at 7.0 -2.1 Å. The final model is superimposed in stick presentation with atoms in standard colors.

interdomain cleft of the Fe^{3+} -soaked form. The two Fe^{3+} -ligating tyrosine residues in the holo form (Tyr 92 and Tyr 191) appear also to participate in the iron coordination in the Fe^{3+} -soaked form, whereas the other two protein ligands of Asp 60 and His 250 are located quite far from the iron atom.

The Structure of the Fe^{3+} Binding Site. The Fe^{3+} binding structure was investigated in more details for the Fe^{3+} -soaked form. Fig. 3a is a stereo diagram of the electron density map calculated with the exclusion of the NTA model *(green, 2Fo - Fc; blue, Fo - Fc)* for the Fe^{3+} -soaked form. The figure clearly demonstrates the existence of iron and NTA close to the Tyr 92 and Tyr 191 ligands.

To evaluate the existence of an iron atom by an alternative way, the author calculated the anomalous difference Fourier density map with exclusion of an iron atom. As shown in Fig. 3b (purple), the existence of iron atom is clearly confirmed by the highest anomalous difference Fourier peak in the density map.

Fig. 4a is a diagram displaying the iron coordination and hydrogen bonding structure in the Fe^{3+} -soaked form. As summarized in Table 2, the distances from the iron of Tyr 92 -OH and Tyr 191 -OH are 1.90 Å and 1.76 Å, respectively, indicating the

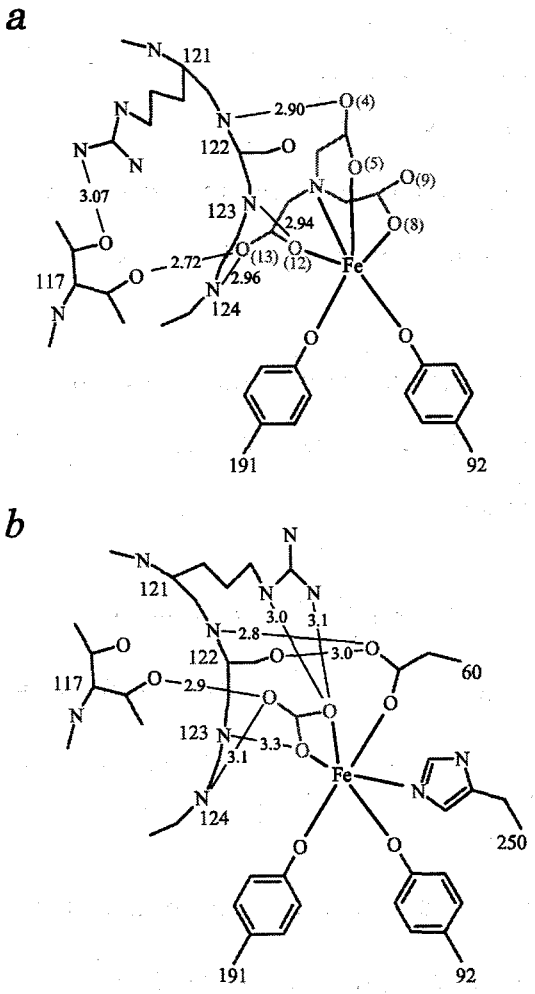

Fig. 4 Diagram of the Fe^{3+} coordination and hydrogen bonding network.

a, the Fe^{3+} -soaked form; b, the holo form. The diagram for the holo form is drawn using the previous data (Kurokawa et al., 1995) for comparison. The thick solid lines in black represent the possible coordination to Fe^{3+}, although the coordination by NTA-N is not clear because of a longer iron to ligand distance (2.76 Å) than the other coordination distances (see Table 2). The thin solid lines in black display hydrogen bonds with the bond distances in Å. The synergistic anions (NTA in a and CO_3^{2-} in b) are shown in light gray. The protein chains are shown in dark gray. The numbers 60 and 250 in b represent Asp 60 and His 250 ligands, respectively.

Fe^{3+} coordination by these two tyrosine residues. The other two protein ligands of Asp 60 and His 250 , however, are not involved in the coordination of the iron atom: the distances of Asp 60 -OD1 and His 250 -NE2 from iron are 9.09 Å and 8.47 Å, respectively. Instead, at least three of the other four Fe^{3+} coordination sites are occupied by NTA; the distances from iron of NTA-O5, NTA-O8, and NTA-O12 are 2.03 Å, 1.73 Å, and 2.22 Å, respectively (Table 2). The last coordination site may be weakly coordinated by NTA-N1 or almost vacant because the distance of this ligand from iron is a slightly larger value of 2.76 Å, compared with the other coordination distances (Table 2). The bond angles formed among NTA-N1, iron, and NTA-O (O5, O8, or O12) are also significantly apart from the ideal 90° (Table 2).

Table 2
Geometry of the iron binding site

Bond lengths (Å)	
Fe-OH (Tyr^{92})	1.90
Fe-OH (Tyr^{191})	1.76
Fe-N1 (NTA)	2.76
Fe-O5 (NTA)	2.03
Fe-O8 (NTA)	1.73
Fe-O12 (NTA)	2.22
Bond angle (degrees)	
OH (Tyr^{92})-Fe-OH (Tyr^{191})	106.5
OH (Tyr^{92})-Fe-N1 (NTA)	157.9
OH (Tyr^{92})-Fe-O5 (NTA)	96.2
OH (Tyr^{92})-Fe-O8 (NTA)	124.7
OH (Tyr^{92})-Fe-O12 (NTA)	96.8
OH (Tyr^{191})-Fe-N1 (NTA)	90.9
OH (Tyr^{191})-Fe-O5 (NTA)	154.1
OH (Tyr^{191})-Fe-O8 (NTA)	87.9
OH (Tyr^{191})-Fe-O12 (NTA)	87.2
N1 (NTA)-Fe-O5 (NTA)	64.2
N1 (NTA)-Fe-O8 (NTA)	68.0
N1 (NTA)-Fe-O12 (NTA)	70.1
O5 (NTA)-Fe-O8 (NTA)	89.2
O5 (NTA)-Fe-O12 (NTA)	77.8
O8 (NTA)-Fe-O12 (NTA)	137.7

The binding of NTA is stabilized through the interactions with the protein chains: NTA-O12 is hydrogen bonded to Ala 123 -N, and NTA-O13, to Thr 117 -OG1 and Gly 124 -N. These protein groups are the ones that form the hydrogen bonds with CO_3^{2-} anion in the holo form (Fig. 4b). As a surprising observation, however, NTA has no direct interaction with the synergistic anion-binding residue, Arg 121 . Another difference in the protein-anion interactions is that the hydrogen bond of NTA-O4 to Ser 122 -N in the Fe^{3+} -soaked form is replaced by that of Asp 60 -OD2 to Ser 122 -N in the holo form.

DISCUSSION

Previous x-ray crystallographic (Bailey et al., 1988; Anderson et al., 1989, 1990; Kurokawa et al., 1995; Rawas et al., 1996, 1997; Moore et al., 1997; Sarra et al., 1990; Dewan et al., 1993; Day et al., 1993; MacGillivray et al., 1998; Jeffrey et al., 1998) and solution scattering (Grossman et al., 1992, 1993; Mecklenburg et al., 1997; Grossmann et al., 1998) analyses have revealed that upon Fe^{3+} uptake, transferrins undergo a large

scale conformational transition from the domain-opened apo structure into the closed holo structure. The structural pathway for the large conformational transition, however, has not been known. The current Fe^{3+} -soaked structure provides crucial information about the structural mechanism for the Fe^{3+} binding.

For loading Fe^{3+} to apotransferrin (apo-Trf), a ferric chelate, most widely ferric NTA (Fe^{3+} ·NTA), is employed (Aisen & Listowsky, 1980). The binding reaction yields a ternary complex consisting of transferrin, Fe^{3+} , and NTA molecules (Trf·Fe^{3+} ·NTA) (Aisen & Listowsky, 1980, Schlabach & Bates, 1975).

$$\text{apo-Trf} + Fe^{3+} \cdot \text{NTA} \rightleftharpoons \text{Trf} \cdot Fe^{3+} \cdot \text{NTA} \quad \text{(Reaction 1)}$$

The Trf·Fe^{3+} ·NTA complex is a stable form in the absence of other synergistic anions. In the presence of a high concentration of bicarbonate, however, NTA is replaced by CO_3^{2-} ; this reaction yields the physiological holo form consisting of transferrin, Fe^{3+} , and CO_3^{2-} (Trf·Fe^{3+} ·CO_3^{2-}) (Aisen & Listowsky, 1980, Schlabach & Bates, 1975).

$$\text{Trf} \cdot Fe^{3+} \cdot \text{NTA} + CO_3^{2-} \rightleftharpoons \text{Trf} \cdot Fe^{3+} \cdot CO_3^{2-} + \text{NTA} \quad \text{(Reaction 2)}$$

The current crystal structure of the Fe^{3+} -soaked form demonstrates essentially the same open conformation as apo-Trf, whereas Trf·Fe^{3+} ·CO_3^{2-} assumes the closed one (Fig. 2). About the implications of the Fe^{3+} -soaked structure for the iron bind-ing pathway, two different mechanisms may be possible.

In the first mechanism, Trf·Fe^{3+} ·NTA assumes the same conformation in solution as the Fe^{3+} -soaked structure, and the total domain closure occurs in Reaction 2. In this

mechanism, the domain closure should depend on the anion replacement. The Trf·Fe^{3+} ·NTA complex shares the two protein ligands (Tyr 92 and Tyr 191 residues) with Trf·Fe^{3+} ·CO_3^{2-} (Fig. 4). Nevertheless, some structural modulations in the iron binding site, other than the protein ligand structures, appear to be highly relevant to the structural mechanism in Reaction 2. As displayed in Fig. 4b,CO_3^{2-} forms hydrogen bonds with Thr 117 -OG1, Ala 123 -N, and Gly 124 -N in the holo form; these protein groups are all hydrogen bonded to carboxylate groups of NTA in the Fe^{3+} -soaked form (Fig. 4a). The protein group Ser 122 -N that forms a hydrogen bond with Asp 60 -OD2 in the holo form also forms a hydrogen bond with NTA-O4 in the Fe^{3+} -soaked form. However, Arg 121 -NE and -NH2 , which are the anchor sites for CO_3^{2-} in the holo form, are both vacant in the Fe^{3+} -soaked form. Such an open situation would be suitable for the subsequent entry of CO_3^{2-} in Reaction 2. My putative pathway for Reaction 2 includes an initial entry of CO_3^{2-} into the Arg 121 anchor sites and then the total replacement of NTA by CO_3^{2-}. This reaction should yield a short lived Trf·Fe^{3+} ·CO_3^{2-} complex with the open conformation, in which only four of the six Fe^{3+} coordination sites are occupied by the protein side chains (Tyr 92 and Tyr 191) and bidentate CO_3^{2-}. As a structural counterpart, the crystal structure of a domain 2 fragment complex, in which all parts of domain 1 as well as the aspartic acid and histidine ligands are deleted by proteolysis, demonstrates the presence of an equivalent Fe^{3+} coordination structure by the two tyrosine residues and CO_3^{2-} (Lindley et al., 1993). The formation of the holo structure is then completed by the coordination of Asp 60 and His 250 ligands to the two vacant Fe^{3+} sites and hence by the domain closure.

In the second mechanism, the Fe^{3+} -soaked form is initially transformed into a closed conformation by the Fe^{3+} coordination of Asp 60 and His 250 ligands, before the

bound NTA molecule is replaced by a carbonate anion. This mechanism, however, requires as a prerequisite the occurrence, in solution, of the differential ternary Trf·Fe^{3+} ·NTA complex with the closed conformation in a carbonate-free condition; the maintenance of the open conformation in the Fe^{3+} -soaked form is accounted for by the arrest due to a crystal packing force from otherwise (free in solution) induced transformation into the closed conformation. The mechanism would also require a rearranged coordination and hydrogen bonding structure for NTA in the Trf·Fe^{3+} ·NTA complex because the Asp 60 and His 250 coordination sites are occupied by NTA in the Fe^{3+} -soaked form (Figs. 3 and 4). As a related observation to the second mechanism, no clear diffraction has been detected for the apo crystal when it is soaked with Fe^{3+} ·NTA in the presence of a high concentration of bicarbonate. This strongly suggests that the apo crystal collapses upon the transformation of the open form into the closed Trf·Fe^{3+} ·CO_3^{2-} . The crystal packing force, therefore, may not be strong enough to arrest the transformation of the open to closed conformation, giving less weight to the second mechanism. At the present stage, however, the second mechanism, which includes a ternary Trf·Fe^{3+} ·NTA complex with a holo-like closed conformation in solution cannot be ruled out because the structure of the Trf·Fe^{3+} ·NTA complex in solution has not been solved.

In conclusion, the previous crystallographic structures of transferrins have been restricted essentially to the two structural forms: one is the domain-opened, iron-free apo form and the other, the domain-closed, Fe^{3+} -loaded holo form (Bailey et al., 1988; Anderson et al., 1989, 1990; Kurokawa et al., 1995; Rawas et al., 1996, 1997; Moore et al., 1997; Sarra et al., 1990; Dewan et al., 1993; Day et al., 1993; MacGillivray et al., 1998; Jeffrey et al., 1998). As an alternative structural state, the current Fe^{3+} -soaked

structure of the ovotransferrin N-lobe is the first demonstration of an Fe^{3+} -loaded, open transferrin form. One of the most important findings in the current structure is that only the two tyrosine residues (Try 92 and Tyr 191) participate in the Fe^{3+} coordination as protein ligands (Figs. 3 and 4 and Table 2). The coordination structure by the two tyrosine residues is consistent with the previous hypothetical structure for the Fe^{3+} -loaded, domain-opened transferrin intermediate (Baker & Lindley, 1992); the hypothetical structure has been derived from the crystallographic data of the iron-loaded domain 2 fragment of duck ovotransferrin in which the Asp and His ligands, but not the two Tyr ligands, are removed by proteolysis (Lindley et al., 1993). Regardless of whether the Trf·Fe^{3+} ·NTA complex assumes the open or closed conformation in solution, the finding that the overall structure of the Fe^{3+} -soaked form is almost indistinguishable from that of the apo form (Fig. 2) is consistent with the view that the two tyrosine residues are the protein ligands for the Fe^{3+} entry in the intact transferrin lobe with the domain-opened conformation.

CHAPTER 3

Crystal Structure of the Apoovotransferrin N-Lobe Bound by Sulfate Anions

In vitro, the release of Fe^{3+} from ferric transferrins requires the presence of a simple anion, such as pyrophosphate, sulfate, and chloride, although the effect of anion on Fe^{3+} release kinetics is significantly different between the two ferric binding sites (Baldwin et al., 1981; Cheuk et al., 1987; Kretchman et al., 1988; Egan et al., 1992; Nguyen et al., 1993; Bailey et al., 1997). The requirement of an anion for Fe^{3+} release has been also demonstrated for the Fe^{3+} - transferrin-receptor complex (Egan et al., 1993). The cellular Fe^{3+} release may, therefore, be regulated by some anion.

Previous kinetic studies have, however, strongly suggested that anion binding to transferrins promotes a structural change of the closed holo form that is an absolute prerequisite for Fe^{3+} release (Kretchman et al., 1988; Nguyen et al., 1993; Cowart et al., 1982, 1986). In the Fe^{3+} -free apo form, all the lobes of iron transporter transferrins assume a conformation with an opening of the interdomain cleft, as revealed by X-ray crystallographic analyses. These structural and functional results imply that the anion-induced Fe^{3+} release by transferrins is closely related to the opening of the domains. The location of the anion binding site which should be crucial knowledge for the understanding of the anion-induced domain opening and iron release mechanism remains, however, to be established.

In the present study, the ovotransferrin N-lobe has been crystallized in an ammonium sulfate solution and the crystal structure has been determined at 1.9 Å resolution by the isomorphous replacement method. The author found the direct

evidence for the presence of three nonsynergistic SO_4^{2-} binding sites (sites 1-3) in the interdomain cleft that is wide open as compared to the holo cleft structure (Dewan et al., 1993). The sulfate anion in site 1 forms hydrogen bonds with an Fe^{3+} -coordinating ligand His250 NE and with Ser91 OG in a hinge strand. The sulfate anion in site 2 partially occupies the synergistic anion binding sites (Arg121 NE and NH2) and is also hydrogen bonded to Ser122 N. In site 3, SO_4^{2-} forms hydrogen bonds with Ser192 OG and N and with Tyr191 N. The functionally important situations of the residues in sites 1 and 2 strongly suggest that anion bindings to these sites play crucial roles for the domain opening and synergistic carbonate anion release in the iron release mechanism of the ovotransferrin N-lobe. A large movement in the side chain orientation of Ser91, when compared between the holo and SO_4^{2-} -bound apo structures, further supports the implications of site 1 for the anion-induced domain opening mechanism.

EXPERIMENTAL PROCEDURES

*Crystallizatio*n. The hen ovotransferrin N-lobe (the N-terminal half-molecule) was isolated and purified as reported by Oe et al. (1988). The apo form of the protein was crystallized using the hanging-drop vapor-diffusion method. The solution in the crystallization drop was prepared, on a silanized coverslip, by mixing 5 μL of a 44.4 mg/mL protein solution [0.05 M Bis-Tris buffer (pH 6.0)] with 5 μL of a precipitant solution [52-53% ammonium sulfate (pH 6.0) and 0.05 M Bis-Tris buffer]. The droplets were equilibrated against 1 mL of the precipitant solution at 20 °C. Crystals were obtained within 1 month.

The apo crystals were subjected to diffraction experiments, using a Nonius precession camera with Ni-filtered CuKα radiation generated by a Rigaku X-ray

generator (40 kV and 20 mA). The precession photographs indicated that the apo crystal belongs to space group $P6_322$ with the following cell dimensions: $a = b = 125.17$ Å and $c = 87.26$ Å.

Data Collection and Processing. Diffraction data were collected using CuKα radiation (λ = 1.5418 Å) with a Bruker Hi-star area detector coupled to a Mac Science M18XHF rotating-anode generator. A total of 194 748 reflections were collected to 1.83 Å resolution. The data were processed, scaled, and merged with Saint (Bruker Analytical X-ray Instruments, Inc., Madison, WI). For multiple isomorphous replacement (MIR), crystals were soaked for 1 h at 20°C in the precipitant solution containing 0.2 mM PCMBS, 2 mM K_2PtCl_4,5 mM $Sm_2(SO_4)_3$, 2 mM HgMeOH, 5 mM $KAu(CN)_2$, 5 mM $Pr(NO_3)_3$, or 10 mM $SmCl_3$. A number of heavy atom derivative data sets were collected and processed in the same way. Only K_2PtCl_4 and $KAu(CN)_2$ derivatives were, however, useable for MIR phasing. Details of the crystal parameter and statistics of the data sets are given in Table 1. One Pt binding site and two Au binding sites were obtained with the difference Patterson method using PHASES. The obtained MIR phase was improved by solvent flattening with PHASES. Statistics of the phasing appear in Table 1. An electron density map was made with the solvent-flattened MIR phase using the data between 15.0 and 3.0 Å. Domains 1 and 2 of the holo form of the ovotransferrin N-lobe (1NNT, 2.3 Å resolution) were translated and rotated to fit the map, respectively, using TURBO-FRODO.

Structure Refinement. The initial model made using the MIR map and the structure of the holo form was refined by simulated annealing with molecular dynamics using a slow-cooling protocol from 3000 to 300 K. This refinement yielded an R of 0.265 for the data between 15.0 and 2.5 Å resolution. Subsequent restrained least-squares

Table 1
Summary of data collection and refinement

Crystal data	
Space group	$P6_322$
Cell dimensions	
a (Å)	125.29
b (Å)	125.29
c (Å)	87.53
V_m (Å^3/Da)	2.7
Molecules/asymmetric unit	1
Observed reflections	188,024
Resolution (Å)	2.09
Independent reflections	24,284
completeness (%)	100
R_{sym} (%)	7.9
Refinement statistics	
Resolution limits (Å)	7.0–2.10
No. of reflections used ($F > 2\sigma(F)$)	20,679
completeness (%)	88.3
No. of protein atoms	2,543
No. of solvent molecules	153
Ions	$3SO_4$/1Fe/1NTA
Final *R* factor	0.189
Free *R* value	0.256
Average *B* factor (Å^2)	22.2
Root mean square deviation from standard geometry	
Bond distances (Å)	0.014
Bond angles (degrees)	3.03
Dihedrals (degrees)	25.0
Improper dihedrals (degrees)	1.37

refinement yielded an *R* of 0.243 for the same resolution. Several rounds of restrained least-squares refinement up to the resolution of 1.9 Å, followed by manual model building, were carried out to improve the model. Four sulfate anions and water molecules having more than 4σ on the *Fo - Fc* map were then added to the model. The alternate side chain positions for the disorders at Asp25, Gln28, Lys100, Arg172, and Lys296 were added to the model in the final step of the refinement. The final model consisted of 329 amino acid residues, four sulfate anions, and 255 water molecules with an *R* value of 0.187 (R_{free} = 0.243) for 27 751 reflections with *F* being greater than 2σ(*F*) between 7 and 1.9 Å resolution (Table 1).

The electron density maps (2*Fo - Fc*, contoured at 1σ) were calculated using the reflection data at 7.0-1.9 Å resolution. The omit maps (*Fo - Fc*, contoured at 3σ) were obtained from the model in which sulfate molecules were excluded.

RESULTS

Quality of the Refined Model. Residues 1-3 are not included in the model, because no clearly interpretable electron density could be seen. To the side chains of residues at positions 25, 28, 100, 172, and 296 were added alternate models to fit the disordered side chains. Relevant refinement statistics are given in Table 1. The overall completeness, R-factor, and R_{free} were 88.1%, 0.187, and 0.243, respectively, for the data where $F > 2\sigma(F)$. For the highest-resolution bin (1.90-1.98 Å), the completeness was 70.2%, and the R-factor and R_{free} were 0.275 and 0.294, respectively. From a Luzzati plot, the mean absolute error in atomic position is estimated to be 0.22 Å.

A Ramachandran plot (Ramakrishnan & Ramachandran, 1965) of the main chain torsion angles is shown in Figure 1. The main chain conformational angles show that about 89.3% lie within the core region, with 99.7% lying within the allowed region. One non-glycine residue (Leu299) lies outside the allowed regions of conformational

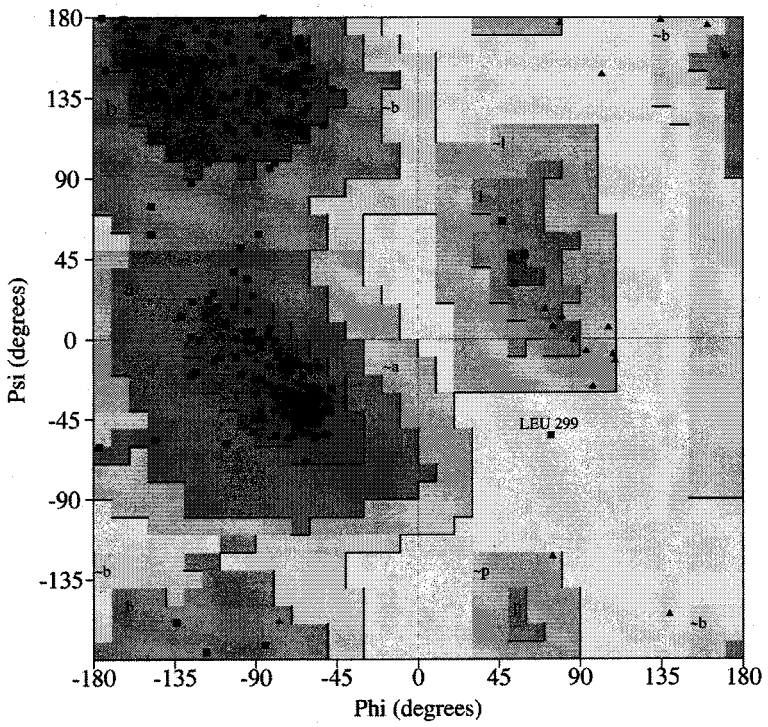

Fig. 1. Ramachandran plot of the backbone torsion angles. Glycine residues are represented by triangles and non-glycine residues by squares. The γ-turn residue, Leu299, is labeled.

space; it is in a γ-turn. The other non-glycine residue (Trp125) lies on the edge of the additional allowed region of α-helix; it is in a distorted α-helix caused by Gly124 and Pro128.

Overall Organization of the Structure. Figure 2 displays the overall structure of the apoovotransferrin N-lobe as a Cα trace. The apo structure, when compared with the previous holo (the Fe^{3+} - and CO_3^{2-} -loaded form) structure of the ovotransferrin N-lobe (Dewan et al., 1993), comprises a domain-opened conformation (Figure 2). The mode and extent of the opening were almost the same as in the N-lobe of the full-length molecule of ovotransferrin (Kurokawa et al., 1999); as calculated by the rigid-body motion method (Gerstein et al., 1993), the domains move 49.7° around a rotation axis passing through the two β-strands linking the domains.

One of the most important observations depicted in Figure 2 is that the bindings of four sulfate anions are clearly detected from an electron density map. Three of the bound anions are located in the interdomain cleft (sulfates 351-353), while the other one (sulfate 354) exists outside the cleft. None of the four anions participated in the intermolecular interactions in the crystal packing. Table 2 summarizes *B*-factors for the

Color figure shown in page 34-a

Fig. 2. Stereo Cα plots of the apo (cyan) and holo forms (red) of the ovotransferrin N-lobe.
The figures were produced with MOLSCRIPT (Kraulis, 1991) and Raster3D (Merritt & Bacon, 1997) as the superimposed ones on domain 2. The holo structure is drawn using the previously determined data (PDB file 1NNT) (Dewan et al., 1993). The residue numbers are labeled for the apo form. The sulfur and oxygen atoms of bound sulfate anions are shown as yellow and red spheres, respectively. Sulfate anions 351-353 correspond to the anions in sites 1-3, respectively.

Table 2
Geometry of the iron binding site

Bond lengths (Å)	
Fe-OH (Tyr^{92})	1.90
Fe-OH (Tyr^{191})	1.76
Fe-N1 (NTA)	2.76
Fe-O5 (NTA)	2.03
Fe-O8 (NTA)	1.73
Fe-O12 (NTA)	2.22
Bond angle (degrees)	
OH (Tyr^{92})-Fe-OH (Tyr^{191})	106.5
OH (Tyr^{92})-Fe-N1 (NTA)	157.9
OH (Tyr^{92})-Fe-O5 (NTA)	96.2
OH (Tyr^{92})-Fe-O8 (NTA)	124.7
OH (Tyr^{92})-Fe-O12 (NTA)	96.8
OH (Tyr^{191})-Fe-N1 (NTA)	90.9
OH (Tyr^{191})-Fe-O5 (NTA)	154.1
OH (Tyr^{191})-Fe-O8 (NTA)	87.9
OH (Tyr^{191})-Fe-O12 (NTA)	87.2
N1 (NTA)-Fe-O5 (NTA)	64.2
N1 (NTA)-Fe-O8 (NTA)	68.0
N1 (NTA)-Fe-O12 (NTA)	70.1
O5 (NTA)-Fe-O8 (NTA)	89.2
O5 (NTA)-Fe-O12 (NTA)	77.8
O8 (NTA)-Fe-O12 (NTA)	137.7

oxygen and sulfur atoms of the four bound anions. The lowest *B*-factors were found for sulfate 351; the values ranged from 37 to 41 $Å^2$ for the five atoms of SO_4^{2-}. The atoms of sulfate 352 exhibited the second smallest values, which ranged from 48 to 52 $Å^2$. Sulfate 353 had slightly larger values, which ranged from 51 to 54 $Å^2$, than sulfate 352. Sulfate 354 exhibited much larger values than the other three sulfate anions; the values ranged from 72 to 75 $Å^2$, suggesting highly mobile and/or a less tight binding nature of SO_4^{2-} located outside the interdomain cleft.

Structures of Anion Binding Sites. Figure 3 displays stereodiagrams of the electron density maps (green, *2Fo - Fc*) for the three sulfate anions located in the interdomain cleft. The figure also shows the omit maps (blue, *Fo - Fc*) calculated with the exclusion-of-sulfate model and demonstrates that three sulfate anions are detected with clear electron densities in the interdomain cleft. As shown in panel a, sulfate 351 exists in proximity to the side chains of His250 and Ser91; I name this anion binding site site 1. Sulfate 352 exists in proximity to the main chain of Ser122 and to the side chain of Arg121, constituting site 2 (panel b). As site 3, sulfate 353 exists in proximity to a main

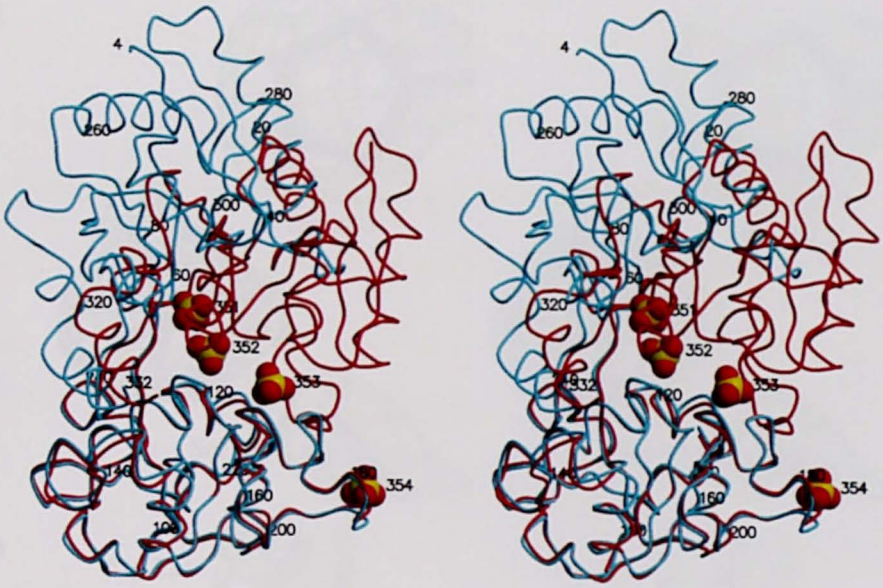
4
280
260
20
300
40
60
50
320
351
352
353
332
120
140
160
200
354

Fig. 2.

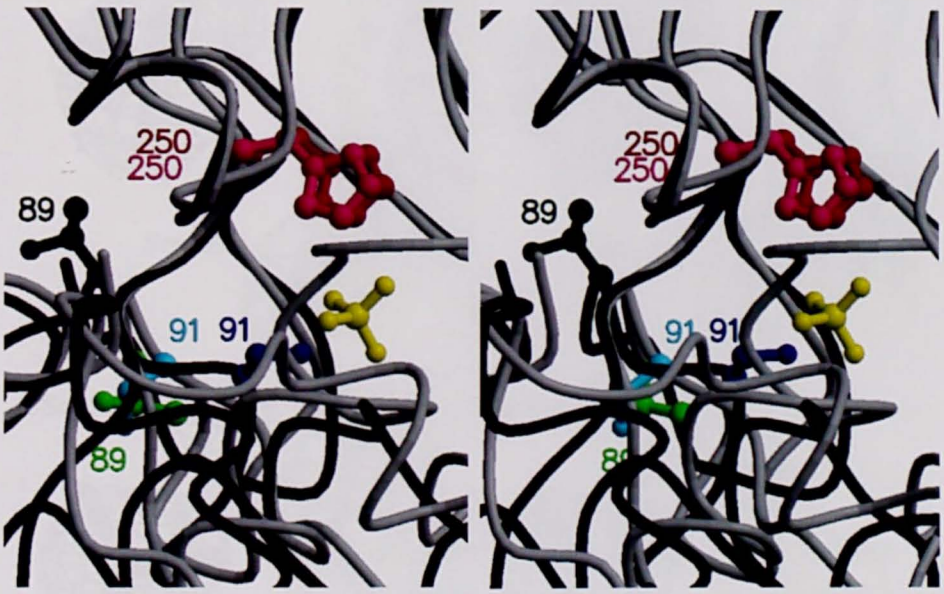
250
250
89
91
91
89

Fig. 5.

Fig. 3.

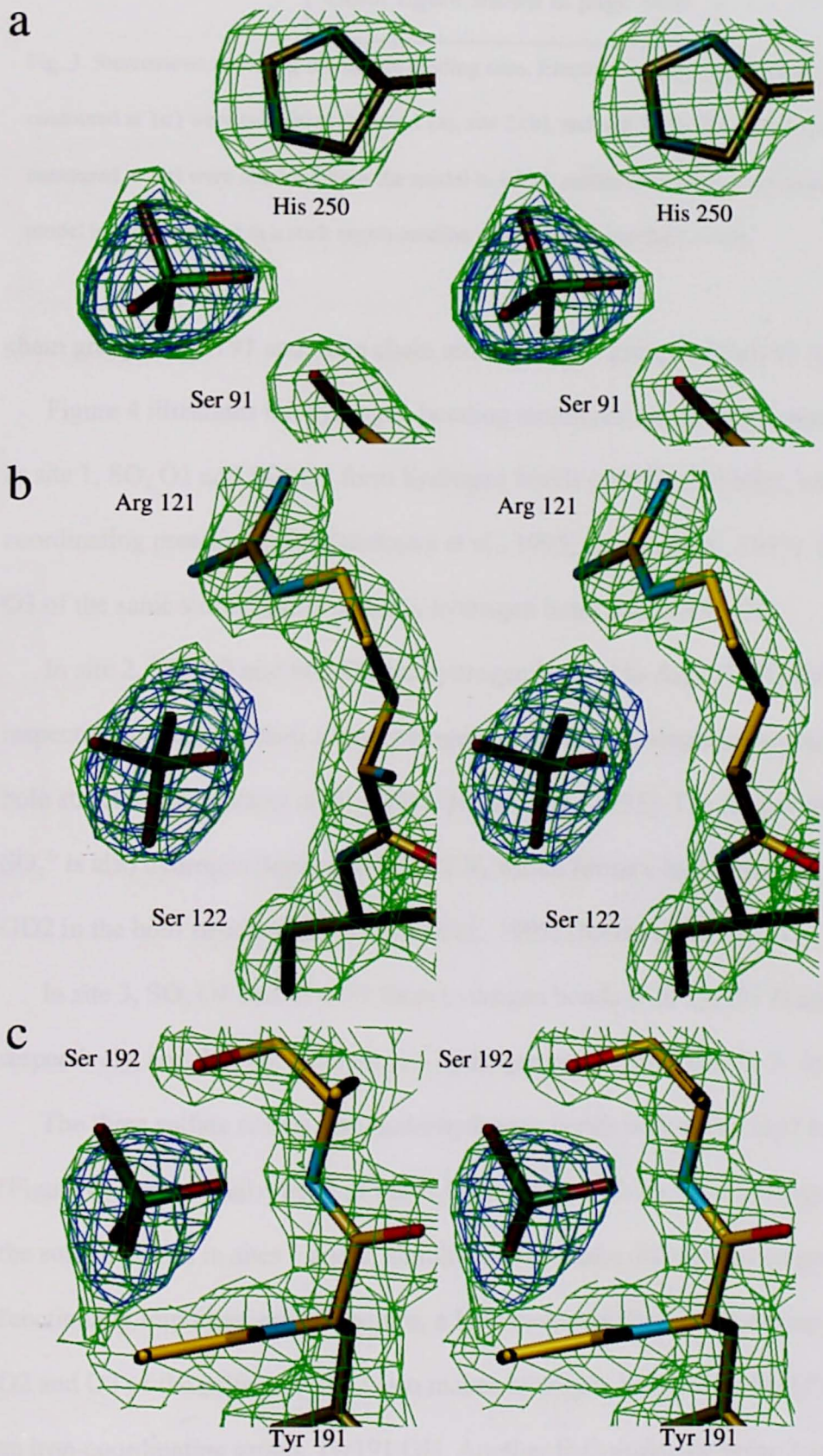
a
His 250
His 250
Ser 91
Ser 91
b
Arg 121
Arg 121
Ser 122
Ser 122
c
Ser 192
Ser 192
Tyr 191
Tyr 191

Color figure shown in page 34-b

Fig. 3. Stereoviews depicting the sulfate binding sites. Electron density maps (green, $2Fo - Fc$, contoured at 1σ) were calculated for site 1 (a), site 2 (b), and site 3 (c). The omit maps (blue, $Fo - Fc$, contoured at 3σ) were obtained from the model in which sulfate molecules were omitted. The final model is superimposed in a stick representation with atoms in standard colors.

chain group of Tyr191 and main chain and side chain groups of Ser192 (panel c).

Figure 4 illustrates the hydrogen bonding structures for the three anion binding sites. In site 1, SO_4 O1 and SO_4 O3 form hydrogen bonds with His250 NE2, which is an iron-coordinating protein group (Kurokawa et al., 1995; Dewan et al., 1993). Oxygen atom O3 of the same sulfate anion makes a hydrogen bond with Ser91 OG.

In site 2, SO_4 O2 and SO_4 O3 are hydrogen bonded to Arg121 NE and NH2, respectively, both of which form hydrogen bonds with synergistic carbonate anion in the holo structure (Kurokawa et al., 1995; Dewan et al., 1993). The former oxygen atom of SO_4^{2-} is also hydrogen bonded to Ser122 N, which forms a hydrogen bond with Asp60 OD2 in the holo structure (Kurokawa et al., 1995; Dewan et al., 1993).

In site 3, SO_4 O4 and SO_4 O1 form hydrogen bonds with Tyr191 N and Ser192 OG, respectively, and SO_4 O2 receives two hydrogen bonds from Ser192 N and Ser192 OG.

The three sulfate anions also make hydrogen bonds with seven H_2O molecules (Figure 4). Interestingly, three of the H_2O molecules, which form hydrogen bonds with the sulfate anions in sites 1 and 2, simultaneously make different hydrogen bonds with functionally important protein groups; a H_2O molecule forming hydrogen bonds with O2 and O3 of the sulfate at site 2 also makes hydrogen bonds with Ser122 N and with an iron-coordinating group, Tyr191 OH. Another H_2O molecule being hydrogen-bonded

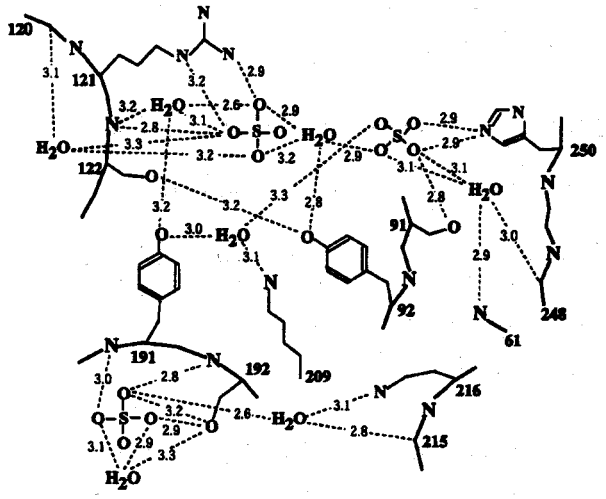

Fig. 4. Diagram of the hydrogen bonding network around the three sulfate anion binding sites in the interdomain cleft. The dotted lines display hydrogen bonds with the bond distances in angstroms.

to O2 of the site 1 sulfate receives hydrogen bonds from an iron-coordinating group, Tyr191 OH, and from a dilysine trigger group, Lys209 NZ. The last H_2O molecule, which forms hydrogen bonds with O3 and O4 of the site 2 sulfate and with O4 of the site 1 sulfate, simultaneously forms a hydrogen bond with another iron-coordinating group, Tyr92 OH.

Surface Accessibilities of the Protein Groups in the Anion Binding Sites. The surface accessibilities of the atoms of the anion binding protein groups of sites 1-3 were calculated and compared with those in the holo structure (Dewan et al., 1993). As summarized in Table 3, all the anion binding atoms exhibited greatly increased

Table 3: Surface Accessibilities of the Atoms in the Anion Binding Sites

	accesibility (Å^2)	
atom	holo form[a]	apo form[b]
site 1		
Ser91 OG	5.99	10.43
His250 NE	0.00	12.09
site 2		
Ser122 N	0.00	5.90
Arg121 NE	0.88	9.68
Arg121 NH2	18.38	50.97
site 3		
Tyr191 N	0.00	3.76
Ser192 N	0.67	2.44
Ser192OG	1.09	28.99

[a] The values were obtained using the previously determined data (PDB file 1NNT) (*17*). [b] For calculation of the accessibility, SO_4^{2-} anions are excluded from the model.

accessibility in the apo structure compared to the holo structure. The three sites are all localized in the Fe^{3+} -binding interdomain cleft. These strongly suggest that the anion binding to these sites is closely related to the domain opening in the ovotransferrin N-lobe.

DISCUSSION

In the study described in this chapter, the apo structure of the ovotransferrin N-lobe has been determined at 1.9 Å resolution with an *R*-factor of 0.187. This model is the highest-resolution structure for the apotransferrins determined to date (Rawas et al., 1997; Jeffrey et al., 1998; Kurokawa et al., 1999; Anderson et al., 1990; Jameson et al., 1998; Sharma et al., 1999) and provides important insight into the iron release mechanism of the N-lobe of transferrins.

The rate for iron release from transferrin is known to be accelerated by several factors, including endosomal low pH (Morgan et al., 1979), association with the specific receptor at acidic pH (Bali et al., 1991), and binding of simple nonsynergistic anions (Baldwin et al., 1981; Cheuk et al., 1987; Kretchman et al., 1988; Egan et al., 1992; Nguyen et al., 1993; Bailey et al., 1997). As an iron release mechanism at low pH from the N-lobes of iron transporter transferrins, the protonation mechanism of the "dilysine trigger" has been proposed on the basis of the ovotransferrin N-lobe holo structure (Dewan et al., 1993); the two lysine residues Lys209 NZ and Lys301 NZ, which are located on the opposite domains of the protein, are separated by only 2.3 Å. This mechanism has been supported by the functional evidence which shows that the rate of iron release from the human serum transferrin N-lobe is much slower in dilysine (Lys206-Lys296) mutants than in the wild-type protein counterpart (Steinlein et al.,

1998; Li et al., 1998; He et al., 1999). According to the apo structure described in this chapter, the Lys209 NZ-Lys301 NZ distance is 7.6 Å. The interaction of the two lysine residues is therefore abolished in the iron-released, domain-opened apo structure, which further supports the dilysine trigger mechanism. As an alternative factor, the requirement of a simple anion or anion chelator for the iron release has been demonstrated either for the N-teminal monoferric serum transferrin (Baldwin et al., 1981; Kretchmar et al., 1988; Egan et al., 1992) and ovotransferrin (Cheuk et al., 1987) or for the isolated N-lobe of serum transferrin (Li et al., 1998; He et al., 1999). Likewise, the iron release from the isolated N-lobe of ovotransferrin is facilitated by the presence of a simple anion, including sulfate anion (Muralidhara, and Hirose, 2000a). Then, a question about whether anion-dependent iron release is directly related to the dilysine trigger mechanism has been raised. Results from the site-directed mutagenesis studies by Woodworth and his collaborators (He et al., 1999; Cheng et al., 1995) have suggested the participation of the dilysine residues as anion binding sites, on the basis of anion titration analyses and Fe^{3+} release kinetics of Lys206 and Lys296 mutants. The results from the ion release kinetics by other laboratories are, however, inconsistent with the view that these two lysine residues are part of anion binding sites for anion-dependent iron release (Steinlein et al., 1998; Li et al., 1998). Such controversial situations have probably been due to the absence of direct structural evidence for nonsynergistic anion binding sites in transferrins.

For the crystallographic analysis of anion binding sites of transferrins, the use of the apo forms is considered appropriate, since the addition of anion to the holo forms should trigger the iron release reaction that accompanies a conformational change. In previous reports, the apotransferrin structure has been determined with the full-length

molecules of lactoferrin (Anderson et al., 1990; Jameson et al., 1998; Sharma et al., 1999) and ovotransferrin (Rawas et al., 1997; Kurokawa et al., 1999), and with the N-lobe of human serum transferrin (Jeffrey et al., 1998). In these studies, crystals have been grown in nonanionic precipitants, including ethanol (Kurokawa et al., 1999), 2-methyl-2,4-pentanediol and ethanol (Jeffrey et al., 1998; Anderson et al., 1990; Jameson et al., 1998), and polyethylene glycol (Kurokawa et al., 1999). Under these precipitant conditions, no attempt has been made to crystallize apo-transferrin saturated with nonsynergistic anion. This study is the first example that utilizes ammonium sulfate as a precipitant for apo crystal growth. The results from this study clearly demonstrate the presence of four bound SO_4^{2-} anions in the apo crystal structure. The absence of bound anion in either Lys209 NZ or Lys301 NZ rules out the direct implication of the dilysine residues for the anion-dependent iron release mechanism. However, a H_2O molecule that makes a hydrogen bond with Lys209 NZ is also hydrogen bonded to coordinating ligand Tyr191 OH as well as to SO_4 O2 of site 1 (Figure 4). Two other H_2O molecules that form hydrogen bonds with the sulfate anions of sites 1 and 2 also make hydrogen bonds with Tyr92 OH and Tyr191 OH (Figure 4). Structural evidence for an iron-loaded open form of the ovotransferrin N-lobe [chapter 2] (Mizutani et al., 1999) demonstrates that Tyr92 OH and Tyr191 OH are the only iron-coordinating protein ligands in an intermediate state of ion binding and release. If the entry of the water molecules into the Tyr groups facilitates iron release, then Lys209 NZ may be indirectly involved in the iron release mechanism. Previous observation (Zak et al., 1995) of decreased iron release rates in a tyrosine-ligand mutant of human serum transferrin (Tyr95His mutation) can be accounted for by this context, if the replacement of the coordinating Tyr with His abolishes the hydrogen bonding network through H_2O molecules.

The current findings that three (sites 1-3) of the four SO_4^{2-} binding sites are all located in the interdomain cleft support more direct participation of anion binding in the iron release mechanism. The surface accessibilities of the protein groups of these sites are greatly increased by domain opening (Table 3). It is therefore very likely that the anion bindings to the three sites stabilize the open conformation. Further-more, structural details strongly suggest that sites 1 and 2 play especially important roles in domain opening and/or release of the synergistic carbonate anion, since these two sites include the protein groups that make functionally important interactions.

Site 1 includes Ser91 OG and His250 NE2. The latter protein group is a consensus Fe^{3+} -coordinating ligand (Bailey et al., 1988; Kurokawa et al., 1995; Haridas et al., 1995; Rawas et al., 1996; Moore et al., 1997; Sharma et al., 1999; Sarra et al., 1990; Dewan et al., 1993; Day et al., 1993; MacGillivray et al., 1998). Furthermore, both Ser91 and His250 are localized in the hinge strands (strands e and j, respectively) (Kurokawa et al., 1995) which can undergo a conformational change upon domain opening and closure. As shown in Figure 5, Ser91 OG faces almost opposite the interdomain cleft and may form a hydrogen bond with Thr89 OG1 with an oxygen-oxygen distance of 3.4 Å in the holo structure (Dewan et al., 1993), but in the apo structure presented in this chapter, the group faces to the cleft and the hydrogen bond is disrupted with an increased Ser91 OG-Thr89 OG1 distance of 10.4 Å. In contrast, the Ser91 OG-His250 NE2 distance, which is 11.9 Å in the holo N-lobe, is shortened to 5.3 Å in the apo form so that these two protein groups interact through a sulfate anion bridge (Figures 4 and 5). Ser91 OG of site 1 has a partially surface accessible nature in the holo structure (Table 3). The Ser91 OG-Thr89 OG1 interaction in the holo structure may be disrupted by the anion binding to the former group, which works as a trigger for

Color figure shown in page 34-a

Fig. 5. Stereodiagrams of site 1 residues. The figures are produced with MOLSCRIPT (Kraulis et al., 1991) and Raster3D (Merritt & Bacon, 1997) as superimposed on 1 domains of the apo and holo structures. The holo structure is drawn using the previous data (PDB file 1NNT) (Dewan et al., 1993). Upper and lower halves are domain 1 and domain 2, respectively, and the right side between the two domains corresponds to the cleft. The apo and holo structures are shown in dark and light colors, respectively: Cα trace in gray, His250 in red, Ser91 in blue, and Thr89 in green. The sulfate molecule is shown in yellow.

the domain opening that includes the above-mentioned structural transition of hinge.

The occupation of site 2 by anion may facilitate both the domain opening and carbonate anion release. Site 2 comprises Ser122 N, Arg121 NE, and Arg121 NH2 (Figures 3 and 4). Arg121 NE and Arg121 NH2 are consensus CO_3^{2-} anchor groups for holotransferrins (Bailey et al., 1988; Kurokawa et al., 1995; Haridas et al., 1995; Rawas et al., 1996; Moore et al., 1997; Sharma et al., 1999a; Sarra et al., 1990; Dewan et al., 1993; Day et al., 1993; MacGillivray et al., 1998). Anion binding to site 2 may therefore facilitate the release of the carbonate anion from transferrin. A protein group, Ser122 N, forms a hydrogen bond in the holo structure (Dewan et al., 1993) with an oxygen atom (OD1) of Asp60; the Asp residue is the only iron-coordinating ligand from domain 1 and plays a central role in domain opening and closure (Grossmann et al., 1993a). The anion binding to site 2 should, therefore, disrupt the Ser122 N-Asp60 interaction, facilitating domain opening. Taken together, it can be reasonably hypothesized that the cooperative anion binding to sites 1 and 2 induces a domain opening and carbonate anion release, and hence iron release.

In conclusion, hypothetical mechanisms for anion-dependent Fe^{3+} release that was

originally proposed by Bates and co-workers (Cowart et al., 1982, 1988) include domain opening and the replacement of CO_3^{2-} by an incoming anion. Although the intensive studies by site-specific mutation analyses have been carried out, the specific residues involved in anion binding have remained largely obscure. The crystal structure described in this chapter provides direct evidence for the anion binding sites in the ovotransferrin N-lobe. Furthermore, the structural details for sites 1 and 2 are closely related to the anion-dependent iron release mechanism in which a domain opening and CO_3^{2-} release are the prerequisites. Although the current anion binding structure is restricted to the case of sulfate anion, sites 1 and 2 comprise the positive charge residues, His250 and Arg121. It is very likely that the basic nature of these sites accommodates the bindings of a wide variety of simple anions.

CHAPTER 4

Domain Closure Mechanism in Transferrins as Deduced from Crystal Structures of Ovotransferrin N-Lobe in Differential Iron-binding States

Most of the large proteins consist of multiple domains (Wodak and Janin, 1981). Upon exertion of biological functions, the multidomain proteins usually undergo significant conformational transition due to the alteration in mutual topological relation of the domains. This is closely related to the structural situations of multidomain proteins that the binding sites of substrates or functional ligands exist between the domains. The X-ray crystal structures of ligand loaded and free forms of multidomain proteins have revealed that the mode of the domain motion can be categorized into two classes: the shear motion and hinge motion mechanisms (Gerstein et al., 1994). The shear motion involves small sliding of domains along multiple interdomain interfaces and the accumulation of many shear movements can result in a large overall motion. The hinge motion mechanism allows the movement of domains as rigid bodies and conformational changes almost lie in hinge regions that link the domains. A typical protein example with this hinge motion mechanism is transferrins (Gerstein et al., 1994).

X-ray solution scattering studies have shown that upon uptake and release of Fe^{3+}, the substantial conformational changes occur in all the three transferrins; the proteins assume open and closed conformations in the apo and holo forms, respectively (Grossmann et al., 1992, 1993a; Mecklenburg et al., 1997). The occurrence of the conformational change by Fe^{3+} binding and release has been confirmed for both the

lobes of ovotransferrin (Kurokawa et al., 1995, 1999) and the N-lobes of human lactoferrin (Jeffrey et al., 1998; Anderson et al., 1989, 1990) and serum transferrin (MacGillivray et al., 1998; Jeffrey et al., 1998) by the X-ray crystallographic analysis. The domain motion in these transferrin lobes follows a common structural mechanism. Domain 2 rotates relative to domain 1 as a rigid body around a screw axis that passes through two β strands linking the two domains. The values of the rotation are 53°, 54° and 63° in the N-lobes of hen ovotransferrin, human lactoferrin, and human serum transferrin, respectively (Kurokawa et al., 1995, 1999; Jeffrey et al., 1998; Anderson et al., 1989, 1990; Sun et al., 1999; Jameson et al., 1998; MacGillivray et al., 1998). In the C-lobe of ovotransferrin, the extent of the rotation is only 35° (Kurokawa et al., 1995, 1999).

For better understanding of the domain motion mechanism in transferrins, the high-resolution crystallographic data in a variety of Fe^{3+}-binding states should be crucial for a transferrin lobe. The author have solved the crystal structure of the apo-form of ovotransferrin N-lobe at 1.9 Å resolution; this resolution is the highest one for the domain-opened transferrin structures solved so far [chapter 3] (Mizutani et al., 2000). In addition, the crystal structure of an iron-loaded but domain opened intermediate at 2.1 Å resolution is at my hand for the same transferrin lobe [chapter 2] (Mizutani et al., 1999). The structure solved for the holo ovotransferrin N-lobe has, however, been restricted to the one at a marginal resolution for detailed conformational transition analyses; the resolutions for the isolated N-lobe (Dewan et al., 1993) and the corresponding lobe in the whole molecule (Kurokawa et al., 1995) are 2.3 and 2.4 Å resolutions, respectively. This has prompted the author to solve the holo structure with an improved resolution. I report the crystal structure of holo ovotransferrin N-lobe at 1.65 Å resolution in this

chapter; this resolution is the one comparable to the so far solved best transferrin data (1.6 Å resolution) of recombinant human serum transferrin N-lobe (MacGillivray et al., 1998).

On the basis of the high-resolution crystal structures of holo- and apo-forms of ovotransferrin N-lobe, the domain motion mechanism has been analyzed in details. The author has also employed the intermediate structure for some analyses including a possible trigger mechanism of the domain motion. The novel points obtained by these analyses are largely related to the hinge structure and motion. First, about the well-known hinge consisting of two antiparallel β strands (first: 89-94, second: 244-249 in ovotransferrin), two of the five main chain hydrogen bonds between the two β-strands clearly undergo hydrogen bond exchanges, which might be closely related to the trigger mechanism for the domain motion. Drastic rearrangements of hydrogen bonding networks are also found in the polypeptide segment (82-94) that includes first β strand, suggesting a 'door closer'-like driving force by the β-strand hinge for the domain motion. As the second point, there exists an alternative hinge that is formed by non-covalent interactions between the two domains. The interactions are multiple van der Waals contacts between domain 1 residue Met331 and domain 2 residues of Trp125, Ile129, and Trp140. This hinge by the van der Waals interactions is placed on a significant distance from the β-strand hinge, thereby securing the correct domain motion. Implications of the new hinge mechanism for other transferrin lobes are discussed on the basis of known crystal structures.

Experimental methods

Crystallization. The N-terminal half-molecule of hen ovotransferrin was isolated, purified and crystallized as described (Oe et al., 1988, Mikami & Hirose, 1990, Dewan et al., 1993).

Data collection and processing. Diffraction data of holo-form was collected using CuKα radiation (λ = 1.5418 Å) with a Siemens Hi-star area detector coupled to Mac Science M18XHF rotating-anode generator. Total of 135,942 reflections were collected to 1.62 Å. The data were processed, scaled and merged with Saint program (Bruker Analytical X-ray Instruments, Inc., Madison, WI). The space group of the holo form

Table 1. Summary of data collection and refinement

A. *Crystal data*	
Space group	$P\ 2_12_12_1$
Cell dimentions	
a (Å)	46.46
b (Å)	85.95
c (Å)	76.10
Vm ($Å^3$/Da)	2.1
Molecules per asymmetric unit	1
Observed reflectios	135,942
Resolution (Å)	1.62
Independent reflections	35,322
completeness (%)	89.0
R_{sym} (%)	5.8
B. *Refinement statistics*	
Resolution limits (Å)	10.0-1.65
No. of reflections used ($I > 2\sigma(I)$)	31,097
completeness (%)	75.3
No. of protein atoms	2,545
No. of solvent molecules	257
Ions	$1Fe^{3+}/1CO_3^{2-}$
Final *R*-factor	0.173
Free *R* value	0.242
Average B-factor ($Å^2$)	18.1
r.m.s. deviation from ideal geometry	
Bond distances (Å)	0.012
Bond angles (deg.)	2.67
Dihedrals (deg.)	24.2
Improper dihedrals (deg.)	1.06

belongs to $P2_12_12_1$ with a cell dimension (Table 1), which is slightly different from the reported crystal (Mikami et al., 1990, Dewan et al., 1993).

Structure refinement. The structure of holo form was refined using the reported model at 2.3 Å resolution (Dewan et al.,1993, PDB 1NNT). The model could be located in the cell by Xplor rigid body refinement using the data between 15.0 Å and 3.0 Å. The model was further refined by simulated annealing with molecular dynamics using a slow-cooling protocol similar to that of Brünger et al. (1989), from 3000 to 300K, and restrained least squares refinement. Several rounds of restrained least squares refinement, followed by manual correction of the model using program TURBO-FRODO, were carried out to improve the model. Water molecules, a CO_3^{2-} ion and a Fe^{3+} ion were added where the difference density had values of more than 3 σ above the mean and the *2Fo-Fc* map showed density at more than the 1 σ level. Final refinement statistics are given in the Table1.

Definition of screw axis. Superposition of structures was carried out using the program FIT (Guoguang Lu, Lund University) and ProFit (SciTech Software). The static cores of domain 1 and domain 2 were identified by a sieve-fit procedure (Lesk et al., 1991). Only Cα atoms were used for the procedure and a 0.45 Å threshold was used. Superposition of static core of domain 2, followed by superposition of domain 1 was carried out. From the equation which superimpose domain 1, screw axis, rotation angle and translation distance were calculated.

Determination of interdomain interactions. Hydrogen bonds were detected using program Quanta and Turbo-FRODO. Two carbon atoms between which distance is smaller than 4.5 Å was determined to have Van der Waals interaction. This calculation was carried out using X-plor.

For determination of the interdomain interactions, a range of domain 1 was defined to be residue 4-91 and 247-332, and a range of domain 2 was defined to be residue 92-246. Hydrogen bonds or van der Waals interactions between the two ranges were determined to be interdomain interactions.

Results

The holo N-lobe structure at 1.65 Å resolution. Residues 1 to 3 are not included in the model, because no clearly interpretable electron density could be seen. To side chains of the residues at 17, 247, 261, 306 and 313, alternate models were added to fit the disordered side chains. Relevant refinement statistics are given in Table 1. From a Luzzati plot, the mean absolute error in atomic position is estimated to be 0.17 Å. Ramachandran plots of the main chain conformational angles shows that about 90.7% lie within the core region, with 99.7% lying within the allowed region. In the plots, one non-glycine residue (Leu299) lies outside the allowed regions of conformational space as in the N-lobe of other transferrins (Jameson et al., 1998; MacGillivray et al., 1998); it is in a γ-turn. The other non-glycine residue (Trp125) lies in the edge of additional allowed region of α-helix; it is in a distorted α-helix caused by Gly124 and Pro128.

Overall organization of the solved holo N-lobe structure at 1.65 Å resolution was essentially the same as those of the previous holo N-lobe structures as the isolated half-molecule at 2.3 Å resolution (Dewan et. al., 1993) and corresponding lobe in the whole molecule at 2.4 Å resolution (Kurokawa et al., 1995). The polypeptide chain is folded into two α/β domains (domain-1 and domain-2) which are linked by two antiparallel β-strand. The Fe^{3+}-binding site is located in the interdomain cleft.

The Fe^{3+}-coordinating structure by four amino acid residues (Asp60, Tyr92, Tyr191 and His250) was almost the same as those of the previous data (Dewan et. al., 1993; Kurokawa et al., 1995) as well. The distance from Fe^{3+} to Asp60-OD1, Tyr92-OH, Tyr191-OH and His250-NE2 are 2.13, 1.87, 1.97 and 2.12 Å, respectively. The electron density map in the present high resolution analysis, however, demonstrates much more clearly the bidentate nature of the carbonate ion ligand; the bond lengths between Fe^{3+} and liganded two oxygen atoms of the carbonate ion (O1 and O3) are 2.06 and 2.09 Å, respectively.

The existence of eight interdomain hydrogen bonds has previously been identified in the N-lobe of diferric whole molecule of ovotransferrin (Kurokawa et al., 1995); Ser122-N...Asp60-OD2, Ser122-OG...Asp60-OD2, Ser122-OG...Tyr324-OH, Asn-126 ND2...Tyr324-OH, Asn185-ND2...Ile12-O, Lys209-NZ...Lys301-NZ, Lys209-NZ...Ser303-OG and Lys296-NZ...Glu215-OE1. Except for the seventh hydrogen bond, the same seven interactions are also found in the present N-lobe structure, in which the existence of four interdomain hydrogen bonds of Tyr92-N...Val247-O, Arg246-NE...Ser91-OG, Lys290-NZ...Asp219-OD1, and Lys296-NZ...Glu215-O is further identified. These eleven hydrogen bonds may help to close the Fe^{3+} binding cleft and may increase stability of the holo-form of ovotransferrin.

Among these interdomain interactions, Lys209-NZ…Lys301-NZ is the dilysine trigger that plays a key role for Fe^{3+} release in an acidic condition (Dewan et al. 1993). The distance between Lys209-NZ and Lys301-NZ that has been shown in the previous report is 2.3 Å. The present high-resolution structure shows a slightly longer distance of 2.8 Å. As previously shown, the two lysine NZ atoms are apart 7.6 Å in the open apo N-lobe structure [chapter 3] (Mizutani et al., 2000).

Mode of the overall domain motion. The obtained holo structure was compared with the previous apo structure at 1.9 Å resolution. Domain 1 and 2 each has a very similar structure in the holo and apo forms, although the cleft formed by the two domains is closed in the holo but wide open in the apo form. To characterize the mode of the domain motion, a method describing movements as 'screw motions' (Gerstein et al., 1993) was used. For this routine, sets of residues, called the 'static cores', in each domain that did not move appreciably with respect to each other were identified by a sieve-fit procedure (Lesk, 1991). A 0.45 Å threshold was adopted and only Cα atoms were used for the procedure. The static cores comprise the residues 5-83, 247-289 and 292-331 in domain 1 and the residues 92-139, 144, 148-176, 178 and 180-245 in domain 2. They include most of the residues of the protein, 93% of domain 1 and 94% of domain 2, which indicates rigid body motion of the domains. When the holo and apo forms are superimposed on the static core of domain 2, the further rotation and translation are required for the superposition of domain 1; the calculated values are 49.7 ° rotation and 2.1 Å translation, around and along a left-handed screw-axis, respectively. The observed overall conformational change is almost the same as the previous data (rotation: 53 °, translation: 1.8 Å) for the N-lobe in the whole molecule of ovotransferrin (Kurokawa et al., 1999), indicating the absence of inter-lobe interaction effects on the overall domain motion.

Motion of individual Cα atoms. Albeit the involvements of most domain residues as the static cores, non-rigid body behavior of other residues may play an important role on the domain motion mechanism. The author investigated how the individual Cα atoms behave upon the domain motion. As a requisite analysis, the distances of Cα atoms to the screw-axis (averaged distances in the holo and apo forms) were plotted. Figure 1

(panel A, green curve) displays the occurrence of four regions along the primary structure that pass very close to the screw-axis; these are the regions consisting of the residues 84-92, 143-144, 247 and 331. The segment His84-Tyr92 and residue Val247 are included in the first and second interdomain peptide segments, respectively; a part of the segment and Val247 are included in the interdomain anti-parallel β-sheet structure. The other two regions, consisting of the residues Ile143-Glu144 and Met331 also exist in a topologically close proximity. In the three-dimensional situation, therefore, there are two regions that are very close to the screw axis.

Figure 1 also displays the topological relation of the individual Cα atoms by the mutual distance (panel A) and by the rotation angles around the screw-axis in the holo and apo forms (panel B). The red and blue curves represent the values upon the superimpositions on the static core of domain 2 and on that of domain 1, respectively. The Cα-Cα distances in the superimposed domain region are very small or almost zero; the Cα-Cα distances in the non-superimposed region show a very similar profile to the distances of the Cα atoms from the screw-axis. These Cα-Cα distance profiles largely reflect the domain motion as a rigid body. We can read from the turnover regions of the

Color figure shown in page 52-a

Fig. 1. Mode of domain motion in ovotransferrin N-lobe.

The distances of Cα atoms to the screw axis were calculated as the averages for the apo and holo forms and are shown along the primary structure by the consecutive green curve (A). For each of the Cα atoms, the extent of motion between the apo and holo forms was estimated as the mutual distance (A) and rotation angle around the screw-axis (B) upon the superposition of the static core of domain 2 (red curve) and of that of domain 1 (blue curve).

red and blue curves in panel A that the boundary of the two domains lies in two regions: the first region comprises multiple residues (residues His84-Ser91) but the second comprises a single residue (Val247). This is more clearly shown by the rotation angle profiles (panel B). In the first region, Cα atoms wobble between the two domains along a long stretch of the residue His84-Ser91, while the second region makes a sharp boundary by a single residue of Val 247. In addition to the domain boundaries, there are two different Cα-wobbling regions consisting of the residues Glu141-Val148 and Met331-Arg332 (panel B), which are mutually localized in a close proximity in the three dimensional structure. Figure 2 displays the difference, between the holo and apo forms, in the torsion angle for the rotation around a virtual Cα-Cα bond. The torsion angle in the residues His84-Ser91 again changes greatly upon the domain motion. The sharp boundary by Val247 can be accounted for by changes in the torsion angels of Cα246-Cα247 (27°) and of Cα247-Cα248 (-37°); these changes are largely accounted

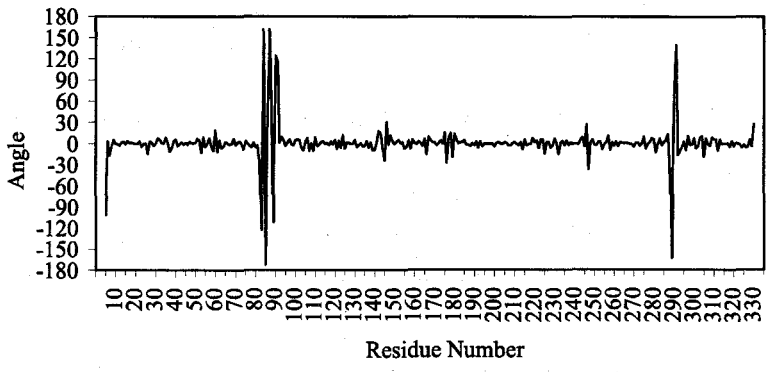

Fig. 2. Difference between the holo and apo forms in the torsion angle around a virtual Cα-Cα bond. Torsion angles for rotations around the virtual bonds connecting Cα atoms were calculated using CNS (Brünger et al., 1998) for the holo and apo forms, and the difference of the two forms was obtained by subtraction of the angle in the holo form from that in the apo form.

Fig. 1.

Fig. 4.

Fig. 5.

Fig. 3.

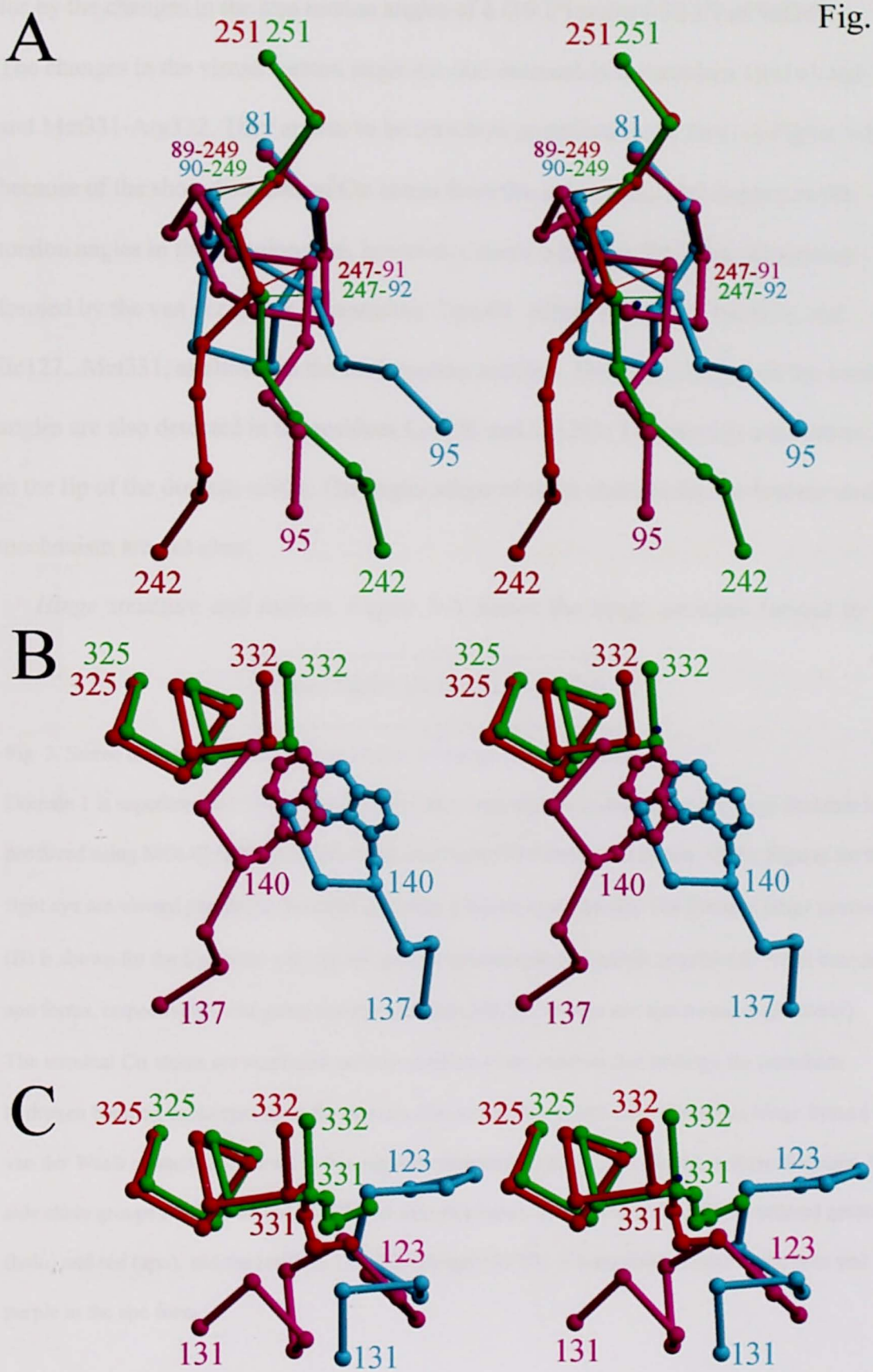
A
251 251
81
89-249
90-249
247-91
247-92
95
95
242
242
251 251
81
89-249
90-249
247-91
247-92
95
95
242
242
B
325
325
332
332
140
140
137
137
325
325
332
332
140
140
137
137
C
325 325
332
332
331
123
331
123
131
131
325 325
332
332
331
123
331
123
131
131

for by the changes in the true torsion angles of ϕ (19.1°) and φ (-33.1°) of Val247. The changes in the virtual torsion angle are also detected in the residues Glu141-Val148 and Met331-Arg332. They appear to be somehow amplified in the form of Figure 1-B because of the short distances of Cα atoms from the screw axis. The changes in the torsion angles in these regions are, however, closely related to the hinge-like nature formed by the van der Waals interactions: Trp140...Met331, Trp125...Met331, and Ile127...Met331, as shown in the forthcoming sections. The large changes in the torsion angles are also detected in the residues Lys290 and Lys291. The two Lys residues exist in the lip of the domain cavity. The implications of these changes for the domain motion mechanism are not clear.

Hinge structure and motion. Figure 3-A shows the hinge structure formed by the

Color figure shown in page 52-b

Fig. 3. Stereo diagrams for the hinge structures in the apo and holo forms.

Domain 1 is superimposed for the apo and holo forms and the stereo diagram of the hinge structure is produced using MOLSCRIPT (Kraulis, 1991) and Raster3D (Merritt and Bacon, 1997). Figures for the right eye are viewed parallel to the screw-axis that is shown by a blue dot. The β-strand hinge structure (B) is shown for the Cα atoms only by the spheres colored cyan and purple (residues 81-95 in holo and apo forms, respectively), and green and red (residues 242-251 in holo and apo forms, respectively). The terminal Cα atoms are numbered and the numbers of the residues that undergo the interchain hydrogen bonding exchanges upon the domain closure are also shown. The alternative hinge formed by van der Waals contacts are shown in two separate diagrams (B and C) for clarity; in these diagrams, the side chain groups for Try140 and Met331 are also displayed. The residues 325-332 are colored green (holo) and red (apo), and the residues 137-142 (B) and 123-131 (C) are colored cyan in the holo and purple in the apo form.

antiparallel β-strands (Thr89-Ala94 and Trp244-Ala249). Although the hinge consists of two β-strands, each strand shows a quite different mode of motion. The latter strand indeed displays an ideal hinge nature: the segments 244-246 and 248-249 behave as a part of the rigid body of domain 2 and that of domain 1, and bend upon the domain closure at Val247. By contrast, the mode of the conformational change in the first β-strand is much more complex. In addition, some exchanges of hydrogen bonds in the β-strands are found as described in details later.

Nine van der Waals contacts were found as the conserved interactions in the holo and apo forms (Table 2). The residues involved in the conserved interactions are Tyr324 and Met331 lying in helix 11 (residues 321-332) of domain 1 and Trp125, Ile127, and Ile129 lying in helix 5 (residues 121-135) of domain 2. The other residue Trp140 exists in the loop region of domain 2 following helix 5. The Cα-Cα distance between Ile127 and Tyr324 is significantly altered upon the domain closure; the difference in the

Table 2. Interdomain Van der Waals contacts
Many interdomain Van der Waals contacts were found in holo- and apo-forms of ovotransferrin N-lobe. Nine of the interdomain contacts were conserved in apo- and holo-forms. In the table, the distance between atoms of the conserved contacts are shown along with Cα-Cα distances between the residues .

Atom in domain 2	Atom in domain 1	distance (Å)		Cα-Cα distance (Å)	
		Holo	Apo	Holo	Apo
Trp125 CD1 ...	Met331 CE	4.1	3.9	10.6	9.7
Ile127 CG1 ...	Tyr324 CE1	4.5	4.2		
Ile127 CD1 ...	Tyr324 CD1	4.1	4.0	9.0	6.6
Ile127 CD1 ...	Tyr324 CE1	3.7	4.1		
Ile129 CB ...	Met331 CE	4.0	4.4	8.8	7.8
Ile129 CG2 ...	Met331 CE	3.7	4.2		
Trp140 CZ3 ...	Met331 CA	4.0	4.2		
Trp140 CZ3 ...	Met331 C	4.5	3.8	9.1	8.8
Trp140 CH2 ...	Met331 C	4.1	4.3		

distances is 2.4 Å between the apo and holo forms (Table 2). In contrast, the Cα-Cα distances between Met331 and the related domain-2 residues (Trp125, Ile129, and Trp140) are almost invariable in the apo- and holo-forms; the differences in the Cα-Cα distances are less than 1.0 Å (Table 2). In addition Met331-CA lies very close to the screw-axis, while Tyr324-CA exists in a significant distance from the axis (see Figure 1-A). These structural features appear to confer hinge-like nature on the non-covalent structure formed by van der Waals interactions of the main chain and side chain groups of Met331 with the side chain group of Trp125, Ile129, and Trp140.

In more details, the distances from the axis of main chain groups Met331-CA and Met331-C, which make van der Waals interactions with Trp140 side chain groups, are 1.3 and 1.0 Å in the apo form, respectively; the corresponding values for the holo form are 0.6 and 0.8 Å. As shown in Table 3, the torsion angles of the Trp140 side chain are almost constant in the apo, intermediate, and holo forms. The hinge mobility can therefore be accounted for by the flexible nature of van der Waals interaction in terms of the bond orientation as displayed by Figure 3-B. By contrast, the distance from the axis of a side chain group Met331-CE, which interact with the side chain groups of Trp125 and of Ile129, is not very short; the distance is 3.6 Å in apo and 3.4 Å in holo structure. The side chain torsion angles of Trp125 and Ile129 are again almost constant upon the domain closure. The torsion angles χ_2 and χ_3 of Met 331 are, however, greatly altered upon the intermediate to holo transformation, hence upon the domain closure (Table 3). That the hinge motion around Met331-CE largely depends on the motion in the side chain torsion angles is displayed as Figure 3-C.

Table 3. Dihedral angles of side chains of residues which participate in second hinge.

Residue	Dihedral	Angle (deg)		
		Apo	Intermediate	Holo
TRP 125	χ_1	-173.7	-173.8	-174.9
	χ_2	-104.7	-100.9	-100.4
ILE 129	χ_1	-62.1	-60.1	-62.6
	χ_{21}	-54.0	-62.1	-45.1
TRP 140	χ_1	-176.0	-178.2	-172.9
	χ_2	67.1	56.7	63.3
MET 331	χ_1	-69.3	-71.6	-74.9
	χ_2	-56.2	-55.8	159.6
	χ_3	-75.3	-77.6	65.6

Hydrogen bonding networks related to the β-strand hinge. Hydrogen bonding networks related to the β-strands or Fe^{3+} binding site in the apo, intermediate and holo forms are shown in Figure 4. Two β-strands of Thr89-Ala94 and Trp244-Ala249 form an antiparallel β-structure which is stabilized by five main chain hydrogen bonds. Three of the five hydrogen bonds (Ala94-O...Trp244-N, Ala94-N...Ala245-O, and Tyr92-O...Val247-N) are retained in all the three transferrin forms. The other two hydrogen bonds, however, undergo crucial exchanges: Ser91-N and Thr89-O, which are, respectively, the hydrogen bonding counterparts of Val247-O and Ala249-N in the open apo and intermediate structures, are replaced by Tyr92-N and Thr90-O in the closed holo structure. As a side chain-related inter β-strand hydrogen bond, the hydrogen bond Thr89-O...Arg246 NH1 formed in the apo and intermediate forms is abolished in the holo form. Instead, the hydrogen bonds Thr89-OG1...Ser91-OG...Arg246 NE are formed in the holo form only (Figure 4). A peptide segment Tyr82-Tyr92, which upon the domain motion, wobbles between the two domains (Figure 1), forms various types of hydrogen bonds, including the ones by main chain-main chain and main chain-side

Color figure shown in page 52-a

Fig. 4. Hydrogen bonding networks related to the β-strand hinge and Fe^{3+} binding site in the apo, intermediate and holo forms.

Hydrogen bonds (dotted lines) and Fe^{3+} coordinations (arrows) found in the holo only (blue), in the holo and intermediate (light green), in the apo and intermediate (red), and in the intermediate only (brown) are displayed. The black dotted lines are the hydrogen bonds conserved in all the three forms. The yellow bar shows the screw axis. The residues conserved in the N-lobes of ovotransferrin, human lactoferrin, and serum transferrin are underlined.

chain interactions. Some side chain groups also form mutual hydrogen bonds through a H_2O molecule (Figure 4). The hydrogen bonding networks in the peptide segment should undergo a drastic rearrangement upon the domain motion, since most of the hydrogen bonds are unique to the open (apo and intermediate) and the closed (holo) structure (Figure 4).

Discussion

In this chapter, the crystal structure of the N-terminal half-molecule of ovotransferrin has been obtained at 1.65 Å resolution. This structure is comparable to the highest resolution transferrin structure solved for the N-terminal half-molecule of human serum transferrin (MacGillivray, et al., 1998). The comparison of the present holo structure with the previous apo [chapter 3] (Mizutani et al., 2000) and intermediate [chapter 2] (Mizutani et al., 1999) structures reveals the detailed domain closure mechanism in ovotransferrin N-lobe. Overall conformational transition follows the common mechanism: the domain 1 and 2 rotate 49.7° as rigid bodies with a translation of 2.1 Å around a left handed screw axis that passes through the two interdomain β-

strands (89-94 and 244-249). As novel observations, the first β-strand undergoes a complex conformational change that includes extensive hydrogen bonding exchanges, although the latter strand bent sharply around at the single residue Val247. The rearrangements of hydrogen bonds may work as a driving force for the domain closure, thereby conferring a 'door closer'-like role, in addition to the canonical hinge role, on the interdomain hinge consisting of the two β-strands. The correct and smooth motion of a door depends on the presence of multiple hinges that mutually separated in a significant distance along a rotation axis. The two β-strands are closely spaced because of their formation of a β-structure and crosses almost perpendicular to the rotation axis (Fig. 3). In this chapter, the author find the presence of an alternative hinge that consists of van der Waals interactions between a domain 1 residue of Met331 and domain 2 residues of Trp125, Ile129, and Trp140. The non-covalent hinge is significantly distant from the canonical β-strand hinge (about 15 Å). Such a dual hinge structure may protect the protein from an aberrant domain motion, including a rotation around an axis that intersects the true axis. The novel domain motion mechanism may generally work in the Fe^{3+} uptake and release in transferrin lobes.

Hinge structure and domain motion in other transferrin lobes. The new hinge motion mechanism shown in this chapter for ovotransferrin N-lobe may be common to all the transferrin lobes. The transferrin lobes that have been solved so far by the crystallographic analysis as set for the closed holo and open apo forms are the N-lobes of human serum transferrin and human lactoferrin and C-lobe of ovotransferrin, in addition to ovotransferrin N-lobe (Hirose, 2000 as review). The author did the same conformational analyses for the three transferrin lobes as for ovotransferrin N-lobe using the known atomic coordinate data. The mode of the overall conformational

transition is essentially the same for the four lobes except for minor differences in the rotation and translation values: in the N-lobes of human lactoferrin, serum transferrin and ovotransferrin and in the C-lobe of ovotransferrin, respectively, the domains rotate around a left handed screw axis with the rotation angles of 54, 64, 50, and 36 degree and with the translations of 0.77, 1.2, 2.1, and 0.47 Å. Figure 5 represents the rotation angles, between the holo and apo forms, of individual Cα atoms around the screw axis in the three transferrin lobes. The patterns are all very similar to the rotation angle pattern in ovotransferrin N-lobe (Fig. 1B); the domain boundary in the first β-strand includes a long stretch of polypeptide segment that undergoes a complex conformational transition, while the boundary in the second β-strand consists of a single hinge residue. The hinge residue in the second β-strand (Val247 in ovotransferrin N-lobe) is conserved in all the lobes: Val 250 in human lactoferrin, Val 246 in human serum transferrin, and Val 589 in ovotransferrin C-lobe.

The participation of non-covalent interactions as the alternative hinge is also found in the N-lobes of serum transferrin and lactoferrin and in the C-lobe of ovotransferrin. The interdomain van der Waals contacts, conserved in the apo and holo forms and found

Color figure shown in page 52-a

Fig. 5. Rotation angles of Cα atoms around a screw axis in the N-lobes of human lactoferrin and human serum transferrin and C-lobe of ovotransferrin.

For each of the Cα atoms, the extent of motion in the N-lobes of human serum transferrin (A) and lactoferrin (B) and the C-lobe of ovotransferrin (C) was estimated as rotation angle around the screw-axis upon the superposition of the static core of domain 2 (red curve) and of that of domain 1 (blue curve) as in Figure 1A.

close to the screw axis, are Thr 122-CG2...Tyr 324-CE1, Thr 122-CG2...Tyr 324-CE2, Thr 122-CG2...Tyr 324-CZ, Trp 138-CZ3...Leu 331-C, and Trp 138-CH2...Leu 331-C in human lactoferrin. Although an interdomain disulfide bond in the N-lobe of human serum transferrin (Cys137-Cys131) and in the C-lobe of ovotranferrin (Cys478-Cys671) is involved in the alternative hinge, the candidate interdomain van der Waals interactions can be found in these lobes as well: Ile130-CD1...Tyr319-CE1, Gly133-CA...Leu326-CD1, Tyr136-CE2...Gly329-C in human serum transferrin N-lobe and Gly469-CA...Leu668-CA, Gly469-CA...Leu668-CB in ovotransferrin C-lobe. The disulfide bond in ovotransferrin C-lobe has little effect on the Fe^{3+} uptake and release function, although the absence of the disulfide bond significantly decrease the conformational stability (Muralidhara and Hirose, 2000b). This might support the crucial implications for the correct domain motion of the van der Waals interactions in the alternative hinge.

Trigger mechanism for the domain motion. The trigger mechanism for the domain motion has been a central question for the transferrin biochemistry. The Fe^{3+}-transporter (serum transferrin and ovotransferrin) and non-transporter (lactoferrin) proteins, however, may not share the common mechanism. As demonstrated by the crystal structures of the apo and holo forms, both the N- and C-lobes of ovotransferrin (Kurokawa et al., 1995, 1999) and the N-lobe (N-half molecule) of human serum transferrin (MacGillivray et al., 1998; Jeffrey et al., 1998) undergo the domain motion between the open and closed conformations. By contrast, both the lobes of mare lactoferrin (Sharma et al., 1999a, 1999b) and the C-lobe of human lactoferrin (Anderson et al., 1990; Haridas et al., 1995; Jameson et al., 1998) assume the closed conformation in either holo or apo crystal structure. This apparent lack of conformational change may

be related to the non-iron-transporting nature, since the open/close mechanism may be crucial for the selective recognition by the receptor of the holo form of a transporter protein (Young et al., 1984; Mason et al., 1987, 1996, 1997). As a possible mechanism for the closed apo structure in lactoferrin, it has been postulated that an equilibrium exists between the open and closed forms of an apo protein in solution, and that the observed closed structure is selected by crystal packing (Anderson et al., 1990).

For human serum transferrin N-lobe, the presence of a trigger mechanism for the domain closure has been claimed by Grossman et al. (1993b) on the basis of the absence, as analyzed by X-ray solution scattering, of the full closure in the Fe^{3+}-loaded Asp63Ser mutant. The residue Asp63 is the only metal coordinating ligand that comes from domain 1. The crystal structure of ovotransferrin N-lobe with Fe^{3+}-loaded, open conformation [chapter 2] (Mizutani et al., 1999) reveals that the initial Fe^{3+} entry site in apo transferrin is two tyrosine residues of Tyr92 and Tyr191, which respectively reside on a hinge strand and domain 2. The trigger model by the coordination of Asp ligand to Fe^{3+}, therefore, appears reasonable on a macroscopic viewpoint. Nonetheless, it is not clear how the Asp residue can travel a long distance of 9 Å [chapter 2] (Mizutani et al., 1999) for approaching the loaded Fe^{3+} onto the two Tyr residues.

The author instead proposes a different trigger mechanism for the domain closure on the basis of the conformational transition mechanism in the β-strand hinge. In this mechanism, an Fe^{3+}-coordinating residue Tyr92 plays a central role. The residue belongs to the first β-strand (89-94), which undergoes the complex conformational change (Figs. 1 and 3) and moves, relative to domain 2, much less than the domain 1 rigid body. The rotation angle and translation of Tyr92-CA are only 16° and 0.46 Å, respectively, while the two domains move mutually 49.7° with a translation of 2.1 Å between the apo and

holo forms. Between the open apo and intermediate forms, no motion is essentially involved between the two domains. Some motion of Tyr92-CA is, however, involved in the apo to intermediate transformation: the motion of Tyr92-CA relative to domain 2 includes the rotation angle of 6 ° and the translation of 0.14 Å. These imply that another motion comprising 10° rotation and 0.32 Å translation is required for the transformation from the open intermediate to the closed holo. The motion of Tyr92-CA upon the apo to intermediate transformation can be accounted for by the indirect interactions between Tyr92-OH and the N-terminal residue groups (Ala123-N and Gly124-N) of helix 5 [chapter 2] (Mizutani et al., 1999) through the introduced Fe^{3+} and synergistic anion (nitrilotriacetate) (Fig. 4). The further Tyr92 motion from the intermediate to the holo may be induced by replacement of the bulky nitrilotriacetate anion by the less bulky synergistic anion, carbonate. This motion may be accompanied by the main chain hydrogen bonding exchanges from Ser91-N...Val247-O and Thr89-O...Ala249-N in the intermediate into Tyr92-N...Val247-O and Thr90-O...Ala249-N in the holo, respectively; these hydrogen bonding exchanges in the interdomain β-structure would further induce the extensive rearrangements in the hydrogen bonding networks in the first interdomain β-strand that would work as a driving force for the domain closure (Figs. 3 and 4). The major point of this domain closure model is that the small triggered motion in Tyr92-CA is amplified as the large conformational transition between the two domains.

The release of Fe^{3+} from ferric transferrins is accelerated in presence of a simple anion, such as pyrophosphate, sulfate, and chloride (Egan et al., 1992; Nguyen et al., 1993; Bailey et al., 1997; Muralidhara and Hirose, 2000a). About the structural mechanism for the anion-dependent Fe^{3+} release, the author has shown the existence of

three sulfate anion binding sites in the inter-domain cleft on the basis of the crystal structure of apo ovotransferrin N-lobe in chapter 3 (Mizutani et al., 2000). As a functionally important site amongst the three sites, a sulfate anion makes direct interactions with Ser 91-OG and His 250-NE2. Both Ser 91 and His 250 are localized in the covalent hinge strands (Figs. 2 and 3) and the former residue is included in the first β-strand that undergoes an extensive conformational change upon the domain motion (Figs.1-3). The residue group Ser 91-OG faces almost opposite to the interdomain cleft [chapter 3] (Mizutani et al., 2000) and forms a hydrogen bond with another hinge-residue group Thr 89-OG1 (Fig. 4) in the holo structure. In the apo structure, however, Ser 91-OG faces to the cleft and the hydrogen bond is disrupted with an increased Ser 91-OG to Thr 89-OG1 distance of 10.4 Å [chapter 3] (Mizutani et al., 2000). In contrast, the Ser 91-OG to His 250-NE2 distance, which is 11.9 Å apart in the holo N-lobe, is shortened into 5.3 Å in the apo form, so that these two protein groups interact through a sulfate anion bridge. Ser 91-OG has partially surface-accessible nature in the holo structure [chapter 3] (Mizutani et al., 2000). The Ser 91-OG to Thr 89-OG1 interaction in the holo structure may be disrupted by the anion binding to the former group, which works as a trigger for the domain opening; the subsequent full domain opening probably utilizes the same structural transition mechanism of the β-strand hinge in the reverse way to the domain closure process.

SUMMARY

The author performed studies on the structural mechanism of iron uptake and release in transferrin by fragmentation and X-ray crystallography of ovotransferrin N-lobe. The findings in each chapter are summarized as follows.

Chapter 1

N terminal fragment (Ala1-Tyr72) of ovotransferrin was prepared. Partially disulfide reduced ovotransferrin N lobe prepared by reduction of ovotransferrin N lobe under non denaturing condition was digested with chymotrypsin and a fragment was purified with ion-exchange chromatography of the digest. From N terminal and C terminal sequence and molecular mass of the fragment, the fragment was assigned to Ala1-Tyr72 of ovotransferrin. CD spectrum of the fragment of revealed that the fragment retained secondary structure; in the conformation of the fragment, digestion with chymotrypsin induced no drastic alteration. This fragment corresponds to N terminal subdomain (N terminal part of domain 1: domain 1N) in ovotransferrin and has a iron-coordinating ligand Asp60.

Chapter 2

Transferrins bind Fe^{3+} very tightly in a closed inter-domain cleft by the coordination of four protein ligands (Asp 60 , Tyr 92 , Tyr 191 , and His 250 in ovotransferrin N-lobe) and of a synergistic anion, physiologically bidentate CO_3^{2-}. Upon Fe^{3+} uptake, transferrins undergo a large scale conformational transition: the apo structure with an opening of the interdomain cleft is transformed into the closed holo structure,

implying initial Fe^{3+} binding in the open form. To solve the Fe^{3+} -loaded, domain-opened structure, an ovotransferrin N-lobe crystal that had been grown as the apo form was soaked with Fe^{3+} -nitrilotriacetate, and its structure was solved at 2.1 Å resolution. The Fe^{3+} -soaked form showed almost exactly the same overall open structure as the iron-free apo form. The electron density map unequivocally proved the presence of an iron atom with the coordination by the two protein ligands of Tyr 92 -OH and Tyr 191 -OH. Other Fe^{3+} coordination sites are occupied by a nitrilo-triacetate anion, which is stabilized through the hydro-gen bonds with the peptide NH groups of Ser 122 , Ala 123 , and Gly 124 and a side chain group of Thr 117 . There is, however, no clear interaction between the nitrilotriacetate anion and the synergistic anion binding site, Arg 121.

Chapter 3

Several lines of functional evidence have shown that anion binding to a nonsynergistic site is a prerequisite for the anion-mediated iron release mechanism of transferrins. The author found structural evidence of the location of sulfate anion binding sites of the ovotransferrin N-lobe via the 1.90 Å resolution apo crystal structure. From the electron density map, the existence of four bound SO_4^{2-} anions was detected. Three of them that exhibited reasonably low *B*-factors were all located in the opened interdomain cleft (sites 1-3). In site 1, the bound anion directly interacts with an Fe^{3+} -coordinating ligand; SO_4 O1 and SO_4 O3 form hydrogen bonds with His250 NE2. Oxygen atom O3 of the same sulfate anion makes a hydrogen bond with Ser91 OG in a hinge strand. The sulfate anion in site 2 partially occupies the synergistic anion binding sites; SO_4 O2 and SO_4 O3 are hydrogen bonded to Arg121 NE and NH2, respectively,

both of which are consensus anchor groups for CO_3^{2-} anion in holotransferrins. The former oxygen atom of SO_4^{2-} is also hydrogen bonded to Ser122 N, which forms a hydrogen bond with Fe^{3+} -coordinating ligand Asp60 OD2 in holotransferrins. Some of the SO_4^{2-} oxygen atoms in sites 1 and 2 interact indirectly through H_2O molecules with functionally important protein groups, such as the other Fe^{3+} -coordinating ligands, Tyr92 OH and Tyr191 OH, and a dilysine trigger group, Lys209 NZ. In site 3, SO_4 O1 and SO_4 O4 form hydrogen bonds with Ser192 OG and Tyr191 N, respectively, and SO_4 O2 forms hydrogen bonds with Ser192 N and Ser192 OG. These structural data are consistent with the view that the anion bindings to the interdomain cleft, especially to sites 1 and 2, play crucial roles in the domain opening and synergistic carbonate anion release in the iron release mechanism of the ovotransferrin N-lobe.

Chapter 4

The crystal structure of holo hen ovotransferrin N-lobe refined at 1.65 Å resolution has been obtained. The comparison of the structure with previous high-resolution apo [Chapter 3] and Fe^{3+}-loaded, domain-opened intermediate [Chapter 2] structures provides new viewpoints about the domain closure mechanism upon uptake of Fe^{3+} in ovotransferrin N-lobe. Overall conformational transition follows the common mechanism: the domains 1 and 2 rotate 49.7 ° as rigid bodies with a translation of 2.1 Å around a screw axis that passes through the two interdomain β-strands (89-94 and 244-249). About the generally believed hinge-like motion of the two strands, the latter strand indeed displays an ideal hinge nature: the segments 244-246 and 248-249 behave as a part of the rigid body of domain 2 and that of domain 1, respectively, and a sharp bent upon the domain closure is largely accounted for by the changes in the torsion angles ϕ

and ψ of Val247. The mode of the conformational change in the first β-stand, however, is much more complex. Two of the five inter β-stand hydrogen bonds undergo crucial exchanges: Ser91-N ... Val247-O and Thr89-O ... Ala249-N in the open apo and intermediate structures into Tyr92-N ... Val247-O and Thr90-O ... Ala249-N in the closed holo structure. These exchanges, which may be triggered in the intermediate state by modulation in the topological relation between the Fe^{3+}-ligated hinge residue Tyr92-OH and the anion anchor residues of helix 5, are accompanied by a large conformational change and extensive hydrogen bonding rearrangements in a long stretch of segment of Glu82 to Tyr92. Such structural transition would work as a driving force for the domain closure, which highlights a 'door closer'- like role, in addition to the canonical hinge role, for the interdomain polypeptide segment pair. As an alternative hinge that secures the correct domain motion by being placed on a significant distance from the β-strand hinge, the author point out the participation of the van der Waals contacts formed between main chain and side chain groups of Met331 in domain 1 and side chain groups of Trp125, Ile129 and Trp140 in domain 2. The screw axis passes very close to Met331-CA and the Cα-Cα distances from Met331 to Trp125, Ile129 and Trp140 are almost constant in the three structural states. The results from the same analyses for the crystal structures of human serum transferrin and lactoferrin suggest that this new hinge mechanism works for other transferrins as well.

ACKNOWLEDGEMENT

The author would like to express his sincere gratitude to Dr. Masaaki Hirose, Professor of the Research Institute for Food Science, Kyoto university, for his pertinent instructions and generous support throughout the course of this study.

The author would like to express special thanks to Dr. Bunzo Mikami, Associate Professor of Research Institute for Food Science, Kyoto University, for his kind help to work and warm encouragement.

The author appreciates Dr. Nobuyuki Takahashi, Research Associate of the Research Institute for Food Science, Kyoto University, for his valuable comments and encouragement.

The author wishes to express grateful acknowledgement to Dr. Honami Yamashita for her kind collaborations and encouragement.

The author wishes to express appreciation to the members of the Research Institute for Food Science, Kyoto University, for their suggestions and worm encouragement.

Finally, the author greatly thanks his family for heartfelt encouragement and support.

REFERENCES

Aisen, P., and Listowsky, I. (1980) *Annu. Rev. Biochem.* **49,** 357-393

Anderson, B. F., Baker, H. M., Norris, G. E., Rice, D. W., and Baker, E. N. (1989) *J. Mol. Biol.* **209,** 711-734

Anderson, B. F., Baker, H. M., Norris, G. E., Rumball, S. V., and Baker, E. N. (1990) *Nature* **344,** 784-787

Bailey, S., Evans, R. W., Garrant, R. C., Gorinsky, B., Hasnain, S., Horsburgh, C., Jhoti, H., Lindley, P.F., Mydin, A., Sarra, R., and Watson, J. L. (1988) *Biochemistry* **27,** 5804-5812

Bailey, C. T., Byrne, C., Chrispell, K., Molkenbur, C., Sakett, M., Reid, K., McCollum, K., Vibbard, D., and Catelli, R. (1997) *Biochemistry* **36**, 10105-10108

Baker, E. N., Rumball, S. V., and Anderson, B. F. (1987) *Trends Biochem. Sci.* **12,** 350-353

Baker, E. N., and Lindley, P. F. (1992) *J. Inorg. Biochem.* **47,** 147-160

Baldwin, D. A., and de Sousa, D. M. R. (1981) *Biochem. Biophys. Res. Commun.* **99,** 1101-1107

Bali, P. K., Zak, O., and Aisen, P. (1991) *Biochemistry* **30**, 324-328

Brünger, A. T., Karplus, M. & Petsko, G. A. (1989) *Acta Crystallog. sec. A*, **45**, 50-61

Brünger, A. T. (1993) *XPLOR Version 3.1: A System for X-ray Crystallography and NMR*, Yale University Press, New Haven

Brünger, A.T., Adams, P.D., Clore, G.M., DeLano, W.L., Gros, P., Grosse-Kunstleve, R.W., Jiang, J.-S., Kuszewski, J., Nilges, N., Pannu, N.S., Read, R.J., Rice, L.M., Simonson, T., and Warren, G.L. (1998) *Acta Crystallog. sec. D* **54**, 905-921

Cheng, Y., Mason, A., and Woodworth, R. C. (1995) *Biochemistry* **34**, 14879-14884

Cheuk, M. S., Keung, W. M., and Loh, T. T. (1987) *J. Inorg. Biochem.* **30**, 121-131

Cowart, R. E., Kojima, N., and Bates, G. W. (1982) *J. Biol. Che*m. **257**, 7560-7565

Cowart, R. E., Swope, S., Loh, T. T., Chasteen, N. D., and Bates, G. W. (1986) *J. Biol. Che*m. **281**, 4607-4614

Day, C. L., Anderson, B. F., Tweedie, J. W., and Baker, E. N. (1993) *J. Mol. Biol.* **232,** 1084-1100

Dewan, J. C., Mikami, B., Hirose, M., and Sacchettini, J. C. (1993) *Biochemistry* **32,** 11963-11968

Egan, T. J., Ross, D., Purves, L. R., and Adams, P. A. (1992) *Inorg. Che*m. **31**, 1994-1998.

Egan, T. J., Zak, O., and Aisen, P. (1993) *Biochemistry* **32**, 8162-8167.

Faber, H. R., Bland, T., Day, C. L., Norris, G. E., Tweedie, J. W., and Baker, E. N. (1996a) *J. Mol. Bio*l. 256, 352-363

Faber, H. R., Baker, C. J., Day, C. L., Tweedie, J. W., and Baker, E. N. (1996b) *Biochemistry* **35,** 14473-14479

Gerstein, M., Anderson, B. F., Norris, G. E., Baker, E. N., Lesk, A. M., and Chothia, C. (1993) *J. Mol. Biol.* **234**, 357-372

Gerstein, M., Lesk, A. M. & Chothia, C. (1994) *Biochemistry*, **33**, 6739-6749

Grossmann, J. G., Neu, M., Pantos, E., Schwab, F. J., Evans, R. W., Townes-Andrews, E., Lindley, P. F., Appel, H., Thies, W.-G., and Hasnain, S. S. (1992) *J. Mol. Bio*l. **225**, 811-819

Grossmann, J. G., Neu, M., Evans, R. W., Lindley, P. F., Appel, H., and Hasnain, S. S. (1993a) *J. Mol. Biol.* **229,** 585-590

Grossmann, J. G., Mason, A. B., Woodworth, R. C., Neu, M., Lindley, P. F., Hasnain, S. S. (1993b) *J Mol Biol.*, **231**, 554-558

Grossmann, J. G., Crawley, J. B., Strange, R. W., Patel, K. J., Murphy, L. M., Neu, M., Evans, R. W., and Hasnain, S. S. (1998) *J. Mol. Biol.* **279,** 461-472

Haridas, M., Anderson, B. F., and Baker, E. N. (1995) *Acta Crystallogr. sec. D* **51**, 629-646

He, Q.-Y., Mason, A. B., Tam, B. M., MacGillivray, R. T. A., and Woodworth, R. C. (1999) *Biochemistry* **38**, 9704-9711

Hirano, H. (1989) *J. Protein Chem.*, **8**, 115-130

Hirose, M. (2000) Bioschi Biotechnol. Biochem., **64**, 1328-1336

Hubbard, S. J. and Thornton, J. M. (1993) 'NACCESS', computer program, Department of Biochemistry and Molecular Biology, University College London

Jameson, G. B., Anderson, B. F., Norris, G. E., Thomas, D. H., and Baker, E. N. (1998) *Acta Crystallogr. sec. D* **54**, 1319-1335

Jeffrey, P. D., Bewley, M. C., MacGillivray, T. A., Mason, A. B., Woodworth, R. C., and Baker, E. N. (1998) *Biochemistry* **37,** 13978-13986

Klausner, R. D., Ashwell, G., van Renswoude, J., Harford, J. B., and Bridges, K. R. (1983) *Proc. Natl. Acad. Sci. U.S.A.* **80**, 2263-2266

Kraulis, P. J. (1991) *J. Appl. Crystallogr.* **24**, 946-950

Kretchmar, S. A., and Raymond, K. N. (1988) *Inorg. Chem.* **27**, 1436-1441

Kurokawa, H., Mikami, B., and Hirose, M. (1994) *J. Biol. Chem.* **269**, 6671-6676

Kurokawa, H., Mikami, B., and Hirose, M. (1995) *J. Mol. Biol.* **254**, 196-207

Kurokawa, H., Dewan, J. C., Mikami, B., Sacchettini, J. C., and Hirose, M. (1999) *J. Biol. Chem.* **274**, 28445-28452

Laskowski, R. A., MacArthur, M. W., Moss, D. S., and Thornton, J. M. (1993) *J. Appl. Crystallogr.* **26,** 283-291

Lee, B. and Lichards, F. M. (1971) *J. Mol. Biol.* **55**, 379-400

Lesk, A. M. (1991) *Protein Architecture: A Practical Approach.* IRL Press, Oxford

Li, Y., Harris, W. R., Maxwell, A., MacGillivray, R. T. A., and Brown, T. (1998) *Biochemistry* **37**, 14157-14166

Lindley, P. F., Bajaj, M., Evans, R. W., Garratt, R. C., Hasnain, S. S., Jhoti, H., Kuser, P., Neu, M., Patel, K., Sarra, R., Strange, R., and Walton, A. (1993) *Acta Crystallogr. Sec. D* **49,** 292-304

MacGillivray, R. T. A., Moore, S. A., Chen, J., Anderson, B. F., Baker, H., Luo, Y., Bewley, M., Smith, C. A., Murphy, M. E. P., Wang, Y., Mason, A. B., Woodworth, R. C., Brayer, G. D., and Baker, E. N. (1998) *Biochemistry* **37,** 7919-7928

Mason, A. B., Brown, S. A., & Church, W. R., (1987). Monoclonal antibodies to either domein of ovotransferrin blook binding to transferrin receptors on chick reticulocytes. *J. Biol. Chem.* **262**, 9011-9015

Mason, A. B., Woodworth, R. C., Oliver, R. W. A., Green, B. N., Lin, L.-N., Brandts, J. F., Savage, K. J., Tam, B. M., & MacGillivray, R. T. A. (1996) *Biochem. J.* **319**, 361-368

Mason, A. B., Tam, B. M., Woodworth, R. C., Oliver, R. W. A., Green, B. N., Lin, L.-N., Brandts, J. F., Savage, K. J., Lineback, J. A., & MacGillivray, R. T. A. (1997) *Biochem. J.* **326**, 77-85

Mecklenburg, S. L., Donohoe, R. J., and Olah, G. A. (1997) *J. Mol. Biol.* **270,** 739-750

Merritt, E. A., and Murphy, M. E. P. (1994) *Acta Crystallogr. Sec. D* **50**, 869-873

Merritt, E. A., and Bacon, D. J. (1997) *Methods Enzymol.* **277,** 505-524

Mikami, B., & Hirose, M. (1990) *J Biochem (Tokyo).*, **108**, 908-908

Mizutani, K., Yamashita, H., Kurokawa, H., Mikami, B., and Hirose, M. (1999) *J. Biol. Chem.* **274**, 10190-10194

Mizutani, K., Yamashita, H., Mikami, B. & Hirose, M. (2000) *Biochemistry*, **39**, 3258-3265

Moore, S. A., Anderson, B. F., Groom, C. R., Haridas, M., and Baker, E. N. (1997) *J. Mol. Biol.* **274,** 222-236

Morgan, E. H. (1979) *Biochim. Biophys. Acta* **580**, 312-326.

Muralidhara, B. K., and Hirose, M. (2000a) *J Biol Chem*; **275,** 12463-12469

Muralidhara, B. K., and Hirose, M. (2000b) *Protein Science*, **9**, 1567-1575

Nguyen, S. A. K., Craig, A., and Raymond, K. N. (1993) *J. Am. Chem. Soc.* **115**, 6758-6764

Nicholson, H., Anderson, B. F., Bland, T., Shewry, S. C., Tweedie, J. W., and Baker, E. N. (1997) *Biochemistry* **36,** 341-346

Oe, H., Doi, E., and Hirose, M. (1988) *J. Biochem.* **103**, 1066-1072

Ramakrishnan, C., and Ramachandran, G. N. (1965) *Biophys. J.* **5,** 909-933

Rawas, A., Muirhead, H., and Williams, J. (1996) *Acta Crystallogr. sec. D* **52**, 631-640

Rawas, A., Muirhead, H., and Williams, J. (1997) *Acta Crystallogr. Sec. D* **53,** 464-468

Sarra, R., Garratt, R., Gorinsky, B., Jhoti, H., and Lindley, P. (1990) *Acta Crystallogr. sec. B* **46**, 763-771

Schagger, H. and Jagow, G. V. (1987) *Anal. Biochem.* **166**, 368-379

Schlabach, M. R., and Bates, G. W. (1975) *J. Biol. Chem.* **250,** 2182-2188

Sharma, A. K., Paramasivam, M., Srinivasan, A., Yadav, M. P., and Singh, T. P. (1999a)

J. Mol. Biol. **289**, 303-317

Sharma, A. K., Rajashankar, K. R., Yadav, M. P., and Singh, T. P. (1999b) *Acta Crystallogr. sec. D* **55**, 1152-1157

Steinlein, L. M., Ligman, C. M., Kessler, S., and Ikeda, R. A. (1998) *Biochemistry* **37**, 13696-13703

Sun, X. L., Baker, H. M., Shewry, S. C., Jameson, G. B. & Baker E. N. (1999) *Acta. Crystallogr. sect. D,* **55**, 403-407

Williams, J., Elleman, T. C., Kingston, I. B., Wilkins, A. G., and Kuhn, K. A. (1982) *Eur. J. Biochem.* **122**, 297-303

Wodak, S. J. & Janin, J. (1981) Location of structural domains in protein. *Biochemistry*, **20**, 6544-6552.

Yamashita, H., Nakatsuka, T, and Hirose, M. (1995) *J. Biol. Chem.* **270**, 29806-29812

Young, S. P., Bomford, A., & Williams, R. (1984) *Biochem. J.* **219**, 505-510

Zak, O., Aisen, P., Crawley, J. B., Joannou, C. L., Patel, K. J., Rafiq, M., and Evans, R. W. (1995) *Biochemistry* **34**, 14428-14434

LIST OF PUBLICATIONS

1. K. Mizutani, H. Yamashita, H. Oe, and M. Hirose: Structural Characteristics of the Disulfide-reduced Ovotransferrin N-Lobe Analyzed by Protein Fragmentation.
   Biosci. Biotech. Biochem. **61** (4), 641-646 (1997).

2. K. Mizutani, H. Yamashita, H. Kurokawa, B. Mikami, and M. Hirose: Alternative Structural State of Transferrin: The Crystallographic Analysis of Iron-loaded but Domain-opened Ovotransferrin N-Lobe.
   J. Biol. Chem. **274** (15), 10190-10194 (1999).

3. K. Mizutani, H. Yamashita, B. Mikami, and M. Hirose: Crystal structure at 1.9 Å Resolution of the Apoovotransferrin N-Lobe Bound by Sulfate Anions: Implications for the Domain Opening and Iron Release Mechanism.
   Biochemistry, **39** (12), 3258-3265 (2000).

4. K. Mizutani, B. Mikami, and M. Hirose: Domain Closure Mechanism in Transferrins: New Viewpoints about the Hinge Structure and Motion as Deduced from High Resolution Crystal Structures of Ovotransferrin N-Lobe.
   Manuscript in preparation.